

國立交通大學
機械工程學系

碩士論文

以 PIC 法模擬場發射電子流之研究

**Analysis of Electron Flows in a Field-Emission Cell Using
Self-Consistent PIC Simulation**



研究生：陳立軒

指導教授：吳宗信 博士

中華民國九十四年七月

以 PIC 法模擬場發射電子流之研究

**Analysis of Electron Flows in a Field-Emission Cell Using
Self-Consistent PIC Simulation**

研究生：陳立軒
指導教授：吳宗信博士

Student : Li-Hsuan Chen
Advisor : Dr. Jong-Shinn Wu

國立交通大學

機械工程學系

碩 士 論 文



A Thesis

Submitted to Institute of Mechanical Engineering Collage of
Engineering

National Chiao Tung University

In Partial Fulfillment of the Requirements

for the degree of

Master of Science

In

Mechanical Engineering

July 2004

Hsinchu, Taiwan, Republic of China

中華民國九十四年七月

誌謝

在交大的日子，感謝吳宗信老師悉心教導，讓我在研究上的能力成長許多，處理事情以及解決問題變得更有效率，同時也感謝口試委員傅武雄教授、郭添全博士在口試時提供的寶貴意見，使得本論文更加充實，在此一併致謝。感謝學長許佑霖、邵雲龍、曾坤樟、連又永、許國賢、李允民、洪捷榮、許哲維、學姊周欣芸在學習上的教導及幫助，感謝同學柏誠、妹吟、東霖在求學中的相互切磋砥礪，以及學弟妹生活上的幫助，使我這兩年的研究生生活非常充實且溫馨。此外，我最愛的親人，由於你們的鼓勵與支持，才使我能在求學的過程中無憂無慮，真的謝謝你們。在這離別的季节裡，大家各奔前程，去追求偉大的夢想，希望大家在不久的將來都能擁有屬於自己的一片天空，我會珍惜一路走來的種種回憶，願大家一切順利。



陳立軒 謹誌

九四年七月于風城交大

以 PIC 法模擬場發射電子流之研究

學生：陳立軒

指導教授：吳宗信

國立交通大學機械工程學系

摘要

場發射顯示器是一種新式平面顯示器，自從奈米碳管被發現以後，它就變的大有可為。場發射顯示技術和一般的陰極射線管電視類似，都是利用電子撞擊螢光粒子引發可見光。在這篇論文裡，利用三維PIC法模擬傳統Spindt型場發射器和奈米碳管場發射器，研究不同的結構和不同的施加電壓所造成的影響。從模擬結果我們可以看出場發射機制確實有遵守Fowler-Norheim規則，奈米碳管和矽基場發射器之間的差異，主要是奈米碳管其高深寬比的幾何形狀所導致較大表面電場會噴出較大的電流。另外，結構裡多了聚焦電極後，電子流發散現象可以有效的改善，在有考慮空間電荷效應，聚焦極施加0伏特，電子散佈在陽極板的寬度將在 $20\mu m$ 範圍內，且絕大多數在 $12\mu m$ 以內。比較有考慮空間電荷效應和沒有考慮空間電荷效應的結果後，可以很明顯地看出場發射電流的差異，其原因是考慮空間電荷效應時，在某一範圍距離內，電子電荷會影響場發射器局部表面電場大小甚鉅。

Analysis of Electron Flows in a Field-Emission Cell Using Self-Consistent PIC Simulation

Student: Li-Hsuan Chen

Advisor: Dr. Jong-Shinn Wu

Institute of Mechanical Engineering
National Chiao Tung University

Abstract

Field emission display is a new type flat-panel display. As carbon nanotubes were discovered, it became the most promising display. FED technology is similar in operation to CRTs in that phosphor is excited by a stream of electrons. In this study, we simulate the traditional Spindt type emitters and nanocarbon emitters by using 3D PIC method to comprehend the influences of structure, and applied field strength on emission current. CNT emitter has larger emission current than silicon-based emitter due to its high aspect ratio geometry. The results show that emission mechanism follows the Fowler-Norheim law. And in focus electrode applied 0 V with space charge effect case, electron dispersion width at anode could decrease effectively within the range of $20\mu m$, and majority is within $12\mu m$. However, it is obviously to see the difference of emission current with/without considering space charge effect, because space charge will influence local surface electric field within a certain distance.

Table of Contents

摘要	I
Abstract	II
Table of Contents	III
List of Tables	IV
List of Figures	V
Chapter 1 Introduction	1
1.1 Motivation	2
1.2 Background	2
1.2.1 Fundamentals of FED	2
1.2.2 Silicon-based Field Emitter	5
1.2.3 CNT-based Field Emitter	6
1.3 Literature Survey	7
1.3.1 FED experiments	7
1.3.2 FED Simulations	9
1.4 Objectives and Organization of the Thesis	10
Chapter 2 Numerical Method	12
2.1 3-D Poisson Equation Solver Using Finite Element Method	12
2.2 3-D Particle Tracing on Unstructured Tetrahedral Mesh	15
2.3 Particle-In-Cell Method (PIC) on Unstructured Tetrahedral Mesh	18
Chapter 3 Results and Discussions	20
3.1 Simulation without Space Charge Effect	20
3.1.1 Simulation of Silicon-based Field Emitter	20
3.1.2 Simulation of CNT Field Emitter	21
3.2 Simulation with Space-Charge Effect	23
3.2.1 Simulation of CNT Field Emitter	23
3.3 Comparison of Simulations with and without Space-Charge Effect	24
3.3.1 Emission current performance	25
3.3.2 Electron trajectory	25
Chapter 4 Conclusions	26
4.1 Summary	26
4.2 Recommendations of the Future Work	27
References	28
Appendix A	33
Appendix B	35

List of Tables

Table I. A FED has excellent features:.....	36
Table II. Classification of FEDs with the structure	37
Table III. Triode-type without space-charge effect (silicon).....	38
Table IV. Triode-type without space-charge effect (CNT 600nm).....	38
Table V. Triode-type without space-charge effect (CNT 400nm).....	38
Table VI. Tetrode-type without space-charge effect (CNT 600nm).....	39
Table VII. Triode-type with space-charge effect (CNT 600nm).....	39
Table VIII. Tetrode-type with space-charge effect (CNT 600nm).....	39



List of Figures

Fig. 1.1 Schematic of the situation at a surface under field emission conditions and the resulting field emission energy distribution.	40
Fig. 1.2 Sketch of a FED performance.	41
Fig. 1.3 The basic structure of triode. A is the substrate, B is the field emitter, C and E the insulating layers, D is the gate and F the anode.	42
Fig. 1.4 The appearance of the 8 in. color FED panel.	43
Fig. 1.5 SEM images of a microcathode.	44
Fig. 2.1 Program flow chart.	45
Fig. 3.1 Contour of the potential distribution around a CNT with a half-ellipsoidal tip. The simulation conditions are: applied voltage 500V, the cathode-to-anode distance $2\mu\text{m}$, radius of the simulation region $1\mu\text{m}$, major radius of the half-ellipsoidal tip 40nm, minor radius of the half-ellipsoidal tip 10nm, CNT radius 10nm, and the total CNT height 100nm.	46
Fig. 3.2 Silicon-based emitter simulation domain. (triode-type)	47
Fig. 3.3 Simulation of silicon-based emitter without space charge effect: (a) is the field emission I-V curve, and (b) shows the data plotted in Fowler-Nordheim coordinates.	48
Fig. 3.4 Typical electron trajectories using PIC simulation without space charge effect (silicon-based emitter without focus electrode): (a) gate applied 160V; (b) gate applied 150V; (c) gate applied 140V; (d) gate applied 130V; (e) gate applied 120V.	49
Fig. 3.5 CNT emitter simulation domain. (triode-type)	50
Fig. 3.6 Simulation of CNT emitter (600nm) without space charge effect: (a) is the field emission I-V curve, and (b) shows the data plotted in Fowler-Nordheim coordinates.	51
Fig. 3.7 Typical electron trajectories using PIC simulation without space charge effect (CNT emitter 600nm without focus electrode): (a) gate applied 160V; (b) gate applied 150V; (c) gate applied 140V; (d) gate applied 130V; (e) gate applied 120V; (f) gate applied 110V.	52
Fig. 3.8 Comparison of emission current of different material emitter. (without space charge effect) ...	53
Fig. 3.9 Comparison of emission current of different emitter height. (CNT emitter without space charge effect)	54
Fig. 3.10 CNT emitter simulation domain. (tetrode-type)	55
Fig. 3.11 Comparison of focusing effect simulations of CNT emitter (600nm) without space charge effect: (a) without focus electrode; (b) focus electrode applied 5V; (c) focus electrode applied 0V; (d) focus electrode applied -5V.	56
Fig. 3.12 Simulation of CNT emitter (600nm) with space charge effect: (a) is the field emission I-V curve, and (b) shows the data plotted in Fowler-Nordheim coordinates.	57
Fig. 3.13 Typical electron trajectories using PIC simulation with space charge effect (CNT emitter 600nm without focus electrode): (a) gate applied 150V; (b) gate applied 140V; (c) gate applied	

130V; (d) gate applied 120V.58

Fig. 3.14 Comparison of focusing effect simulations of CNT emitter (600nm) with space charge effect:
(a) without focus electrode; (b) focus electrode applied 0V.....59

Fig. 3.15 Space charge distribution, left hand side is the full view and right hand side is the local
magnification: (a) electron just leaving emitter; (b) simulation domain full of electrons.....60

Fig. 3.16 Comparison of emission current simulations of CNT emitter (600nm): with (hollow) and
without (solid) space charge effect.....61

Fig. 3.17 Typical electron trajectories using PIC simulation (CNT emitter 600nm): (a) without space
charge effect, without focus electrode and gate applied 150V; (b) with space charge effect,
without focus electrode and gate applied 150V; (c) without space charge effect, focus applied 0V
and gate applied 150V; (d) with space charge effect, focus applied 0V and gate applied 150V. ..62



Chapter 1 Introduction

Field emission display (FED) is a new type of flat-panel display in which electron emitters, arranged in a grid, are individually controlled by “cold” cathodes to generate colored light. FED technology is similar in operation to CRTs in that phosphor is excited by a stream of electrons traveling through a vacuum (from the cathode to the anode). Unlike CRTs, FEDs have no cathode heater. Instead of thermionic emission, electrons are emitted by a cold pixel electron source that typically consists of a large array of low-work-function emitter microtips. And CRTs use a single beam that must be steered by a power-inefficient deflection system. Thus, FEDs could provide the high image quality of today’s CRT displays, require less power than today’s CRT displays, and really achieve the flat-panel display. When compared with TFT LCDs, FEDs offer a superior viewing angle and are several microseconds quicker in response time. Moreover, because of the cold cathode emission, instant-on is available at wide temperature extremes (-40 to 85°C), and the potential for high brightness and contrast is possible. Therefore, field emission flat panel displays seem to be especially promising in becoming a strong competitor to liquid crystal displays. Table I. shows the excellent features of FEDs and Table II. shows the classification of FEDs with the structure [Itoh et al., 2004].

1.1 Motivation

In FED design, the goal is to achieve lower driving voltage and higher light efficiency. Utilize computer simulation code to assist the design of geometry of diode or triode and the arrangement of emitter array in order to obtain larger current density in the low-voltage operation. And design focus electrode to consider electrons spread. Due to the space charge effect occurring at high emission currents, the program must be time domain for self-consistent of the electric field and the charged particles. In comparison of the difference between time domain with space charge effect and without space charge effect, find out the importance of self-consistent of the electric field and the charged particles. Considering the shape of emitters, numerical method of this study takes the advantage of finite element method to construct more flexible meshes. In addition, when the simulation model is in practically dimension, more computing sources are required, and computer simulation code must be parallelized. Finite element method is suitable for parallelizing.

1.2 Background

1.2.1 Fundamentals of FED

Emission means the release of electrons from parent atoms. Most obviously we have emission from the solid into the vacuum, the electron overcoming the work

function barrier in the process. However, a high electric field near the emitter can be sufficient to lower the barrier, so the surface potential step confining the electrons to the solid becomes a triangular shaped barrier. Close to the surface the shape of the barrier is influenced by the image charge potential. Under the conditions depicted the tunneling probability of electrons close to the Fermi energy is large enough to let them escape into vacuum [Gröning et al., 2000]. This is (cold) field emission. Fig. 1.1 shows above descriptions.

FEDs utilize the fundamentals of field emission. A FED removes electrons from the cathode, and makes them collide with fluorescent material applied to the anode, thus emitting light (Fig. 1.2). While the cathode of a CRT uses a point electron source, a FED uses a surface electron source. Normally, electrons are emitted from a cathode that is heated (thermionic emission). As field emission, the electric field (E) plays a similar role to the temperature in thermionic emission, and the governing equation is derived in 1928 by Fowler and Nordheim [Fowler et al., 1928]. The generally accepted Fowler-Nordheim theory for a clean metal surface relates the field emission current density, J , to the electric field at the surface, E , in volts/cm and the work function, ϕ , in electron volts (eV) by the equation

$$J = \frac{AE^2}{\phi^2(y)} \exp\left(-B \frac{\phi^{3/2}}{E} v(y)\right) \frac{A}{cm^2}, \quad (1.1)$$

where

$$A = 1.5414 \times 10^{-6}, \quad (1.1a)$$

$$B = 6.8309 \times 10^7, \quad (1.1b)$$

$$y = 3.79 \times 10^{-4} E^{1/2} / \phi. \quad (1.1c)$$

y is the image charge lowering contribution to the work function. The functions $t(y)$ and $v(y)$ are approximated by $t^2(y) = 1.1$, $v(y) = 0.95 - y^2$.

Typically, the field emission current I is measured as a function of the applied voltage V and we can substituted $J = I / \alpha$ and $E = \beta \frac{V}{d}$ in Eq. (1.1), where α is the emitting area, β is the local field enhancement factor, V is the applied voltage and d is the vacuum gap in the field emission diode configuration. Combining these relationships gives

$$I = aV^2 \exp\left(\frac{-b}{V}\right), \quad (1.2)$$

where

$$a = \frac{\alpha A \left(\frac{\beta}{d}\right)^2}{1.1\phi} \exp\left[\frac{B(1.44 \times 10^{-7})}{\phi^{1/2}}\right], \quad (1.3)$$

$$b = \frac{0.95B\phi^{3/2}}{\frac{\beta}{d}}. \quad (1.4)$$

From Eq. (1.2) we can find out the emitting current is related to the magnitude of applied voltage, the emitting area, and the work function. Using Eq. (1.2) and dividing both sides with V^2 and taking nature log into both sides, it can in turn be written as

$$\ln\left(\frac{I}{V^2}\right) = -\frac{b}{V} + \ln a. \quad (1.5)$$

Hence, a Fowler-Nordheim plot of $\ln(I/V^2)$ versus $1/V$ gives a straight line, and is a good check on the field emission mechanism if it does indeed follow the F-N law.

1.2.2 Silicon-based Field Emitter

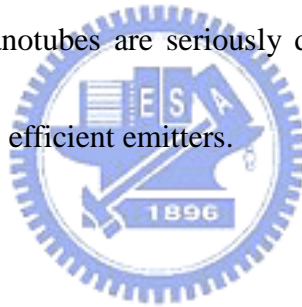
Since 1928 Fowler and Nordheim had studied the phenomenon of electron field emission and mentioned the governing equation, there was not any application in microelectronics until Shoulders proposed [Shoulder, 1961] for the first time the use of a “field emitter” as the electron source, consisting of sharpness points of suitable material in 1961. Because of their sharpness, they could locally enhance the electric field originating from an externally applied voltage to the point of causing electron emission. In 1968 Spindt created micron-sized metallic tips [Spindt, 1968]. The basic structure of the vacuum triode (Fig. 1.3) [Iannazzo, 1993]: a field emitter “cathode” generates electrons, the flow of which is controlled by a “gate” before they are collected by the “anode”, to which the accelerating potential is applied. The triode structures are attractive because a low-voltage operation is achieved due to placing the “gate” electrode close to the tip and making the radius of the tip very small. The low voltage of operation of these cathodes makes them less vulnerable to damage by ionization of the ambient gas [Iannazzo, 1993]. Hence, the low voltage allows the cathodes to operate continuously with very stable emission properties and long life. It

was showed evidence of a subsequent gradual decline of emission performance with time, amounting to about 10% in 7000 h of total life [Spindt et al., 1976]. Furthermore, Spindt type field emitter arrays are up-to-now the only industrially viable film field emitters.

1.2.3 CNT-based Field Emitter

Multiwalled (MWNT) and singlewalled (SWNT) carbon nanotubes were discovered respectively in 1991 [Iijima, 1991] and 1993 [Iijima et al., 1993]. They can be metallic as well as semiconducting, depending on the tube geometry [Wildoer et al., 1998; Odom et al., 1998]. They show promising prospects for applications: they are mechanically extremely stiff and resistant to bending [Falvo et al., 1997], and their suitable as a tip for scanning probe microscopy has also been demonstrated [Dai et al., 1996]. They furthermore had been proven to be very good electron field emitters [Heer et al., 1995; Collins et al., 1997; Bonard et al., 1998; Wang et al., 1997; Rao et al., 2000] and were shown to provide high currents at relatively low operation voltages with good stability. Carbon nanotubes (CNTs) compare well to other film emitters primly because of their high aspect ratio [Bonard et al.], which results in large field enhancement factor. Other strong points of carbon nanotube emitters are the possibility of their relatively simple production in very large quantities (in 1 g of pure nanotube material we can expect in the order of 10^{16} nanotubes, each having a

field enhancement factor of about 1000) and their chemical inertness [Gröning et al., 2000]. The chemical inertness of carbon field emitters especially is one of the most important advantages over silicon or metal microtips, which suffer emission degradation due to sputter erosion and chemical contamination and therefore require a high vacuum environment for operation. After a comparative study of field emission from carbon nanotubes, Bonard et al. [Bonard et al.] concluded that the nanotubes should be multiwalled and have closed, well graphitized tips to obtain good performances as well as long emitter lifetimes. Furthermore, quite surprisingly, the emission characteristics of nanotubes are seriously degraded by opening their ends and opened tubes were far less efficient emitters.

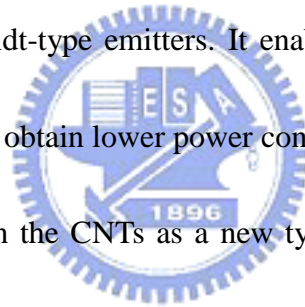


1.3 Literature Survey

1.3.1 FED experiments

Dr. Meyer of LETI presented the capability of using Spindt-type emitters for a display [Meyer et al., 1986]. This proposal became the trigger of the start of the development of field emitters as electron sources of displays by researchers and electronics makers in 1990. Currently, the development stage of Spindt-type FEDs with Mo emitter is close to an end. The monicolor Spindt-type FEDs are being supplied to the market, and the color FEDs are ready for mass production (Fig. 1.4)

[Itoh, 2004]. At the initial stage of development of FEDs the degradation of emission was the most important issue. It has already reported that the emission characteristic is influenced by the quality of atmospheric gas [Itoh et al., 1993]. A FED is degrading proportional to its lifetime, and could be recovered to that of the initial status by baking [Itoh, 2004]. This result shows that the main cause of emission degradation is the phenomenon of gas absorption and not a structural change of the emitter cones. For low voltage drivers of Spindt-type emitters, it is well known that reducing the diameter of gate holes is effective. By the decrease of the diameter could realize the high-density small sized Spindt-type emitters. It enables the Spindt-type emitters to drive with low voltage, and to obtain lower power consumption [Itoh, 2004].



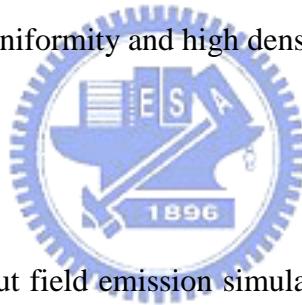
Recently, the research on the CNTs as a new type of the field emission source has become active. A fully sealed field-emission display 4.5 in. in size has been fabricated using SWNT [Choi et al., 1999]. The fabricated CNT-FED showed unusually high brightness at low operating voltage (1800 cd/m^2 at $3.7 \text{ V}/\mu\text{m}$), compared that of Spindt-type FEDs (300 cd/m^2 at 6kV). And it was observed that SWNT films showed higher emission uniformity and current density than MWNT. In 2002 Pirio et al. [Pirio et al., 2002] published CNT field emission microcathodes with an integrated gate electrode (Fig. 1.5) and the device achieved truly low-voltage field emission. They concluded that in order to obtain reproducible emission characteristics

and to avoid degradation of the device, it was necessary to operate the gate in a pulsed voltage mode with a low duty cycle. In the future, they hope to fabricate a single CNT per gate because the screening effect is observed when many CNTs are in close proximity, thus lowering the effectiveness of the applied field [Nilsson et al., 2000].

However, there are some problems presently using CNT to be FED source as follows [Itoh, et al., 2004]:

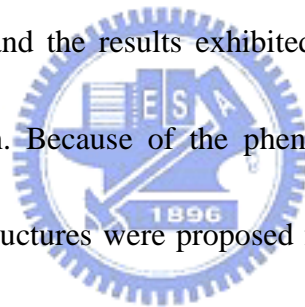
- (a) difficult to form the nanotubes perpendicular to the substrate,
- (b) necessary to remove the residual material like binder,
- (c) difficult to keep the good uniformity and high density of the emission sites.

1.3.2 FED Simulations



In 1990s most researches about field emission simulation neglected the space charge effect [Hong et al., 1994; Wang et al., 1997; Lei et al., 1998]. Hong et al. concluded that the actual electron emission area of a tip in a single or multiemitter structures are related to tip radius, geometry factor, and interemitter interactions. Wang et al. simulated a disk-edge field emitter and the advantageous results are greater emission current, back-ion-bombardment protection, when it is compared to point-like microemitters. Moreover, the distribution of the emission current can be influenced by the gate thickness. Lei et al. mentioned more emitters did not necessarily lead to high emission current and the presence of the gate can reduce the interaction of field

between neighboring tips in the triode structure. Although we could obtain some information, there was no adequately accuracy in the spatial electric field without considering the space charge effect, because electrons released from cathode emitters will form an electron cloud near cathode that could constrain further electrons moving from emitters. For this reason, Hu [Hu et al., 2003] used MAGIC to simulate the field emission properties. MAGIC is a finite-difference code that calculates self-consistently electromagnetic field including the space charge effect, which is very important for high emission current situations. In the same way, Lan [Lan et al., 2004] simulated new triode mode and the results exhibited the gate voltage had a strong effect on display's resolution. Because of the phenomenon of spread of emission electrons, several focusing structures were proposed for field emission devices, such as the coaxial-type focusing, the coplanar-type focusing, and the ridge-type focusing. Lan [Lan et al., 2000] study which type is suitable for display application.



1.4 Objectives and Organization of the Thesis

Based on previous reviews, the current objectives of the thesis are summarized as follows:

- (1) To verify the 3D FE program by means of comparing with available data.
- (2) To study field emission current in triode-type structure and focusing effects in tetrode-type structure.

(3) To compare the difference of simulation results between silicon-based emitter and CNT.

(4) To contrast simulations with and without space-charge effect.

The organization of the thesis would be stated as follow: First is this introduction, and next is the numerical method. Then show the results and discussions. Finally summarize and recommend the future work.



Chapter 2 Numerical Method

This study uses a particle-in-cell computer simulation code which is developed by Kuo-Hsien Hsu, MUST, NCTU. The simulation code is three-dimensional, finite-element, time domain for self-consistent of the electric field and the charged particles. General flowchart of the field emission simulation in a vacuum space is shown in Fig. 2.1. We will briefly describe this flowchart as follows. First, Distribution of initial static electric field (E) due to applied external voltage at cathode is solved by Poisson equation. Using this initial E field, we then continue our PIC method, F-N equation and field equation repeated solving process. In the following, we will describe the details of first 3-D Poisson solver using finite element method, then 3-D particle tracing on unstructured tetrahedral mesh and finally the PIC method.

2.1 3-D Poisson Equation Solver Using Finite Element Method

We begin with an introduction of the Finite Element Method (FEM) that identifies the broad context of the subject [Burnrtt, 1987]:

The FEM is the computer-aid mathematical technique for obtaining approximate numerical solution to the abstract of calculus that predict the response of physical system subjected to the external influences.

Such problems arise in many area of engineering, science, and applied

mathematics. Applications to date have occurred principally in the areas of solid mechanics, heat transfer, fluid mechanics, and electromagnetism. New areas of application are continually being discovered, recent ones include solid-state physics and quantum mechanics.

The salient features in FEM include the following:

1. The domain is divided into smaller regions called elements. Adjacent elements touch without overlapping, and there are no gaps between the elements. The shapes of the elements are intentionally made as simple as possible.
2. In each element the governing equations, usually in differential or variational (integral) form, are transformed into algebraic equation. The element equations are algebraically identical for all elements of the same type, which usually need to be derived for only one or two typical elements.
3. The resulting numbers are assembled (combined) into a much larger set of algebraic equations, which are called the system equations. In the process of element assembly, boundary conditions can be enforced automatically. Such huge systems of equations can be solved economically because the matrix of coefficients is “sparse” in essence.
4. Resulting matrix equation is then solved using suitable efficient matrix solver.

FEM seeks an approximate solution \tilde{U} , an explicit expression for U , in terms of

known, functions, which approximately satisfies the governing equations and boundary conditions. It obtains an approximate solution by using the classical trial-solution procedure.

Construction of a trial solution:

$$\tilde{U}(x; a) = a_0 + a_1 N_1(x) + a_2 N_2(x) + \dots + a_n N_n(x) \quad (2.1)$$

where x is the independent variable in the problems. The functions $N(x)$ are known functions called trial functions (basis). The coefficients, a , are undetermined parameters called degree of freedom (DOF).

We apply FEM to solve Poisson equation. The purpose is to determine specific numerical value for each parameter a_i . In this FEM, we employ Galerkin weighted residual method. For each parameter a_i we require that a weighted average of $R(x; a)$ over the entire domain be zero. The weighting functions of the Galerkin weighted residual method are trial functions $N(x)$ associated with each a_i .

$$\int R(x; a) N_i(x) dx \quad (2.2)$$

3-D Poisson Equation Solver

Poisson equation can be written as follows,

$$\nabla^2 \varphi = -\frac{\rho}{\varepsilon_0} \quad (2.3)$$

By applying Galerkin weighted residual method using C^0 -linear shape functions, on *tetrahedral* mesh, after some algebra [Appendix A] the resulting final matrix equation

can be formulated as follows:

$$\begin{bmatrix} K_{11}^{(e)} & K_{12}^{(e)} & \cdots & K_{1n}^{(e)} \\ K_{21}^{(e)} & K_{22}^{(e)} & \cdots & K_{2n}^{(e)} \\ \vdots & \vdots & \cdots & \vdots \\ K_{n1}^{(e)} & K_{n2}^{(e)} & \cdots & K_{nn}^{(e)} \end{bmatrix} \begin{bmatrix} a_1 \\ a_2 \\ \vdots \\ a_n \end{bmatrix} = \begin{bmatrix} F_1^{(e)} \\ F_2^{(e)} \\ \vdots \\ F_n^{(e)} \end{bmatrix}$$

where

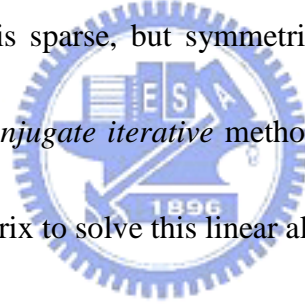
$$K_{i,j}^{(e)} = \frac{1}{36V^2} \varepsilon \iiint (b_i^* b_j^* + c_i^* c_j^* + d_i^* d_j^*)^{(e)} dx dy dz$$

$$F_i^{(e)} = -(\varepsilon \iint \phi_i^{(e)} \tau_u^{(e)} dA + \iiint \phi_i^{(e)} \rho dx dy dz)$$

$$\varphi^{(e)}(x, y, z; a) = \sum_{j=1}^4 a_j \phi_j(x, y, z)$$

$$\phi_i(x, y, z,) = \frac{1}{6V} (a_i^* + b_i^* x + c_i^* y + d_i^* z)$$

Since the coefficient matrix is sparse, but symmetric and positive define, we have applied the *preconditioned conjugate iterative* method [Saad, 1996] and use *random pack* to store the resulting matrix to solve this linear algebra equation.



2.2 3-D Particle Tracing on Unstructured Tetrahedral Mesh

The particle tracing [Lian, 2001] is performed cell-by-cell in unstructured grids taking the advantage of cell connectivity provided by the unstructured mesh data. The first step of the particle tracing is to determine whether the particle will across if the particle will stay in or leave the current cell. If the particle leaves, then the second step is to determine the intersection poison on the intersecting face. Further journey of the particle depends on the face condition. If it is the normal face between cells, then it will continue its movement until the time step ends. If the intersection face is an I/O

boundary, the particle will be removed. If not, then process the interaction according to the wall boundary conditions. Related procedures are described next.

Without considering the external force effects, position of traced particle at $t + \Delta t$ can be written as

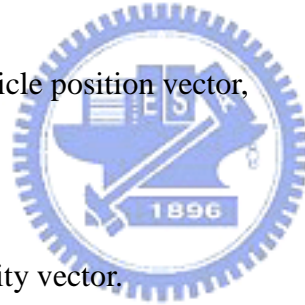
$$\bar{P}_f(t) = \bar{P}_i + \bar{V} \cdot \Delta t, \quad (2.4)$$

where

$$\bar{P}_f(t) = \begin{pmatrix} x \\ y \\ z \end{pmatrix} = \text{final particle position vector}, \quad (2.4a)$$

$$\bar{P}_i(t) = \begin{pmatrix} x_i \\ y_i \\ z_i \end{pmatrix} = \text{initial particle position vector}, \quad (2.4b)$$

$$\bar{V} = \begin{pmatrix} u \\ v \\ w \end{pmatrix} = \text{particle velocity vector}, \quad (2.4c)$$



On the other hand, cell face can be represented as a planar equation as

$$\bar{n} \cdot \bar{p} + d = 0, \quad (2.5)$$

where $\bar{n} = (a, b, c)$ is normal unit vector of the face and $\bar{p} = (x, y, z)$ is the position vector.

By solving eqn. (2.4) and (2.5), we have

$$\Delta t' = \frac{-(ax_i + by_i + cz_i + d)}{(au + bv + cw)} \quad (2.6)$$

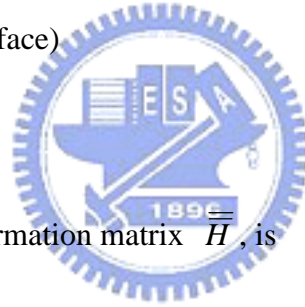
Computing (2.6) of each face in the current cell in turn and the current

intersecting face number is identified by finding the minimum positive $\Delta t'$, the intersection position of the intersecting face of the cell is also found by substituting $\Delta t'$ into eqn. (2.4). If the intersecting face is a normal face between cells, then continue its trajectory until it stops.

If the intersection face is a solid face, the particle will be reflected diffusively or specularly. Both of the two conditions are processed by the transformation between the local coordinate system (on the face) and the absolute coordinate system. First, a unit vector \bar{x}' along the face is chosen, then \bar{y}' is the cross product of \bar{x}' and \bar{z}'

(the normal unit vector of the face)

$$\bar{y}' = \bar{z}' \times \bar{x}' \quad (2.7)$$



The coordination transformation matrix $\bar{\bar{H}}$, is

$$\bar{\bar{H}} = \begin{bmatrix} \bar{x}' \\ \bar{y}' \\ \bar{z}' \end{bmatrix} \quad (2.8)$$

Furthermore, due to the orthonormal set of \bar{x}' , \bar{y}' and \bar{z}' , so the inverse transformation $\bar{\bar{H}}^{-1}$ can be written as

$$\bar{\bar{H}}^{-1} = \bar{\bar{H}}^T, \quad (2.9)$$

where $\bar{\bar{H}}^T$ is the transpose matrix of $\bar{\bar{H}}$.

Now, the particle velocity can be transformed from the absolute coordinate system velocity (\bar{V}_{abs}) to the local coordinate system velocity (\bar{V}_{loc}) before the

reflection by using $\overline{\overline{H}}$.

$$\overline{V}_{loc} = \overline{\overline{H}} \overline{V}_{abs} \quad (2.10)$$

After the reflection of the particle, the new local coordinate system velocity (\overline{V}'_{loc}) can be written as

$$\overline{V}'_{loc} = F(\overline{V}_{loc}, \text{wall condition}), \quad (2.11)$$

where $F(\overline{V}_{loc}, \text{wall condition})$ is a kernel function, and wall condition is the solid wall boundary condition.

Finally, the absolute velocity after the reflection (\overline{V}'_{loc}) will be obtained by using

the inverse transformer H^{-1}

$$\overline{V}'_{abs} = \overline{\overline{H}}^{-1} \overline{V}'_{loc} = \overline{\overline{H}}^T \overline{V}'_{loc} \quad (2.12)$$

Then, the particle continues its journey with its new absolute velocity until it stops.

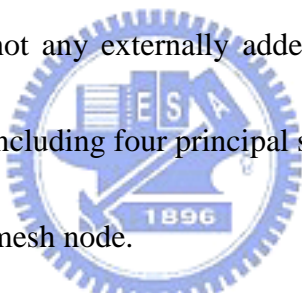


2.3 Particle-In-Cell Method (PIC) on Unstructured Tetrahedral Mesh

The PIC method [Birdsall, 1985] was originally designed for collisionless charged particle simulation. It models the movement of charged particles under the influence of Lorentz force ($F = q(E + v \times B)$, q : particle charge, E : electric field, B : magnetic field) and solves the field equations (Maxwell or Poisson equation) due to redistribution of charge density () and charge current (J) at each time step. A mesh is introduced to sample the space charge and current distributions that center the field

equation. The sampling is performed by appropriate *charge assignment* from the particle locations to the grid points. Afterward, the computed fields (E & B) from field equations at grid points are *interpolated* back to the charge-particle positions. Then, charged particles are moved their new positions using the concept of *Boris rotation* [Birdsall, 1985] without actually computing the forces explicitly. This process repeats itself to obtain the self-consistent solution during the simulation. This is so-called **particle-in-cell (PIC)** method.

In this study we calculate Lorentz force only considering electric field (E), because we assume there is not any externally added magnetic field (B). Now, we repeated PIC method orderly including four principal steps:

- 
- (1) Assign charge to the mesh node.
 - (2) Solve the field equation on that mesh.
 - (3) Calculate the mesh-defined force field.
 - (4) Interpolate to find forces on the particles.

By solving the field equation using finite element method, the interpolation between grid and charge particles comes naturally from the numerical method (FE) itself.

Chapter 3 Results and Discussions

We have verified our Poisson solver with previously published simulation data by Hu, under the same conditions of the current study. Hu used a commercial code, Magic, to obtain the potential distribution around the tip and we have extremely similar results in Fig. 3.1. Next we proceed to simulate different structures, such as triode and tetrode, and different material emitters with silicon based and CNTs. Then the emission current and focusing effect are compared and analyzed. However, the most important matter we have to explain is why we must consider space charge effect.



3.1 Simulation without Space Charge Effect

In this section, we only solve Poisson equation one time, and use the initial E field repeated in the solving process. Other simulation procedure is proceeding by time step (10^{-16} second).

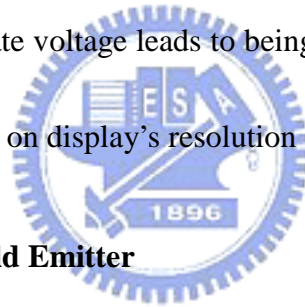
3.1.1 Simulation of Silicon-based Field Emitter

Fig. 3.2 shows the detail simulation domain and illustrates the geometry dimension. We simulate a quarter FED cell $x \times y \times z = 25 \mu m \times 25 \mu m \times 50 \mu m$. The half gate aperture is $0.5 \mu m$. The silicon-based emitter height is $1 \mu m$, the tip radius is

10 nm, and half-angle θ is 20° . So far as to boundary condition, anode and cathode are given constant voltage (Dirichlet), and on the other side is chosen Neumann. The work function here chooses 4.5eV .

3.1.1.1 Applied field strength effects

The voltages applied on anode and cathode, are 400V and 0V , respectively. And we change gate electrode voltage from 120V to 160V . Fig. 3.3 shows the I-V curve and its Fowler-Nordheim plot of $\ln(I/V^2)$ versus $1/V$ gives a straight line, so the field emission mechanism followed the F-N law certainly. From the results of electron trajectory (Fig. 3.4), higher gate voltage leads to being more dispersive. For these, the gate voltage has strong effects on display's resolution and emission current.



3.1.2 Simulation of CNT Field Emitter

Fig. 3.5 exhibits the whole simulation conditions almost same as silicon case. It just substitutes the emitter with CNT and changes the height of gate electrode close to the tip. But the work function here we choose 5.0eV for CNT.

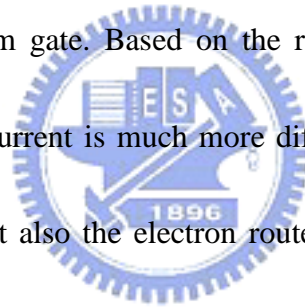
3.1.2.1 Applied field strength effects

The voltages applied on anode and cathode, are 400V and 0V , respectively. And we change gate electrode voltage from 110V to 160V . Fig. 3.6 shows the I-V curve and its F-N plot also gives a straight line. The simulation results also have the trend higher gate voltage gives greater dispersion width (Fig. 3.7), and we can notice larger

current in CNT model than in silicon-based model at the same applied field (comparison shown in Fig.3.8). We could assume it is due to CNT its high aspect ratio geometry because the strength of electric field around the sharp edge is stronger than that around small curvature surface. Despite silicon-based emitter has lower work function, CNT emitter still renders more current by its larger surface electric field.

3.1.2.2 CNT height effects

Considering the effect of CNT height, we can see the difference from the I-V curve plot (Fig. 3.9). Higher emitter produces higher emission current, and it depends on the distance tip apart from gate. Based on the results, when applied voltage is strengthened, the extractive current is much more different between cases of 400nm and 600nm. Not only this but also the electron route. There will be some electrons impacting the gate electrode resulting in the reduction of anode current at 400nm case.



3.1.2.3 Focusing effects

In order to improve the resolution when a stream of electrons excite phosphor, we add a focus electrode to gather electron flows, a coaxial tetrode-type, and the simulation conditions are shown in Fig. 3.10. The half focus aperture is chosen $1.5\mu m$ to decrease interception of electrons. Also, the gap between gate electrode and focus electrode should not be too large based on the test case experience, because higher focus electrode position will obstruct more electrons moving toward anode. It

is apparently to see focusing effect from the electron trajectory picture (comparison shown in Fig. 3.11). However, the focus electrode must be given appropriate voltage to get optimum electron flows that means phosphor is excited by its aligned electron source. When focus electrode is applied over-biased voltage, the electrons flow will spread again, and electrons exiting from anode will decrease. Here, the focus electrode applied 0 V performs better than ± 5 V. As the result of 0 V, electron dispersion width at anode is within the range of $13\mu m$, and majority is within $10\mu m$.

3.2 Simulation with Space-Charge Effect

In this section, we solve Poisson solver once per 50 time steps to consider space charge effect.



3.2.1 Simulation of CNT Field Emitter

The simulation domain is identical to 600nm case of simulation without space-charge effect. Then we could compare the results with and without space-charge effect.

3.2.1.1 Applied field strength effects

Anode and cathode are applied 400 V and 0 V, respectively. Gate voltage is applied 150 V, 140 V, 130 V, and 120 V to observe field strength effects. The results (see Fig. 3.12) tell us it follows the F-N law, and also the tendency of greater

dispersion width (Fig.3.13) and more emission electrons as applied larger gate voltage (Table VII.).

3.2.1.2 Focusing effects

We take focus 0 V for example. Fig. 3.14 shows the comparison of with and without focusing effect. With focus electrode, electrons spread within the range of $20\mu m$, and most within $12\mu m$.

3.3 Comparison of Simulations with and without Space-Charge

Effect

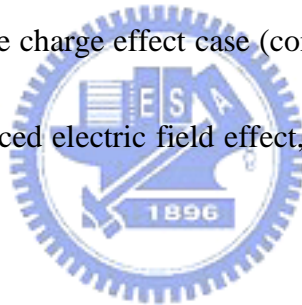
There will be local normal electric field changing if we consider space charge effect. We could see the electrons distribution causes the variation of local electric field on emitter surface from Fig. 3.15. Fig. 3.15 (a) shows the first electron leaves its parent cell atom. The maximum normal electric field is 10.00152 V/nm that is a bit difference to 10.00628 V/nm without space charge, but the local surface electric field is influenced and the difference amount is up to 7.249065 V/nm. However, as far as Fig. 3.15 (b), despite it is filled with electrons, but the distance electron apart from emitter surface is reached enough magnitude, the difference amount of local surface electric field is just 1.0509998E-02 V/nm in maximum. So we can make a conclusion that space charge will influence local surface electric field within a certain distance.

3.3.1 Emission current performance

It is obviously to see the difference of emission current with/without considering space charge effect (Fig. 3.16), because current density is dependent on local electric field. Based on above conclusion we have made, the emission current is deeply influenced by local surface electric field as electron just leaving its parent atom.

3.3.2 Electron trajectory

Whatever triode-type or tetrode-type, the electron trajectory plot is a little more dispersive in considering space charge effect case (comparison shown in Fig. 3.17). It could be thought as the advanced electric field effect, electron moving based on field force right away.



Chapter 4 Conclusions

4.1 Summary

The current study carries out the simulations of triode-type and tetrode-type field-emission cell using self-consistent PIC method, and the major findings of the current research are summarized as follows:

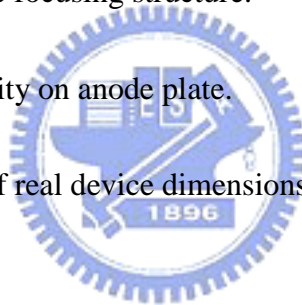
1. Gate voltage has strong effects on display's resolution and emission current.
2. CNT emitter has larger emission current than silicon-based emitter due to its high aspect ratio geometry.
3. Emitter tip as close to gate electrode as it could is better.
4. Focus electrode must be applied appropriate voltage to get optimum electron flows. In focus electrode applied 0 V with space charge effect case, electron dispersion width at anode is within the range of $20\mu m$, and majority is within $12\mu m$.
5. Whether simulation proceeds with space charge effect or not, it will follow the F-N law.
6. Space charge will influence local surface electric field within a certain distance.
7. It is obviously to see the difference of emission current with/without considering space charge effect.

8. The electron trajectory plot is a little more dispersive in considering space charge effect case because of the advanced electric field effect, electron moving based on field force right away.


4.2 Recommendations of the Future Work

Based on this study, future work is suggested as follows:

1. To test time step effect in a shorter interval to investigate the present result if it achieves adequately accuracy.
2. To simulate coplanar-type focusing structure.
3. To study the current density on anode plate.
4. To carry out simulation of real device dimensions if possible.



References

1. Birdsall, C.K. and Langdon, A.B., *Plasma Physics via Computer Simulation*, Mc Graw-Hill, New York, NY, USA (1985).
2. Bonard, J.-M., Maier, F., Stockli, T., Chatelain, A., Heer, W. A., Salvetat, J.-P., and Forro, L., “Field emission properties of multiwalled carbon nanotubes,” *Ultramicroscopy* **73**, 7 (1998).
3. Bonard, J.-M., Salvetat, J.-P., Stöckli T., Forro, L., and Chatelain, A., “FIELD EMISSION FROM CARBON NANOTUBES: A COMPARATIVE STUDY.”
4. Burnett, David S., *Finite Element Analysis from Concepts to Application* (1987).
5. Choi, W. B., Chung, D. S., Kang, J. H., Kim, H. Y., Jin, Y. W., Han, I. T., Lee, Y. H., Jung, J. E., Lee, N. S., Park, G. S., and Kim, J. M., “Fully sealed, high-brightness carbon-nanotube field-emission display” *Appl. Phys. Lett.* **75**, 3129 (1999).
6. Collins, P.G. and Zettl, A., “A simple and robust electron beam source from carbon nanotubes,” *Appl. Phys. Lett.* **69**, 2679 (1996).
7. Dai, H., Hafner, J. H., Rinzler, A. G., Colbert, D. T. and Smally, R. E., “nanotubes as nanoprobe in scanning probe microscopy,” *Nature* **384**, 147

- (1996).
8. Falvo, M. R., Clary, G. J., Taylor II, R. M., Chi, V., Brooks JR, F. P., Washburn, S., and Superfine, R., "Bending and buckling of carbon nanotubes under large strain," *Nature* **389**, 582 (1997).
 9. Fowler, R. H., and Nordheim, L., "Electron Emission in Intense Electric Fields," *Proc. Roy. Soc. A (London)* **119**, 173 (1928).
 10. Groning, O., Kuttel, O. M., Emmenegger, Ch., Groning, P., and Schlapbach, L., "Field emission properties of carbon nanotubes," *J. Vac. Sci. Technol. B* **18**, 665 (2000).
 11. Heer, W. A., Chatelain, A., and Ugarte, D., "A Carbon Nanotube Field-Emission Electron Source," *Science* **270**, 1179 (1995).
 12. Hong, D., and Aslam, M., "Simulations of fabricated field emitter structures," *J. Vac. Sci. Technol. B* **12**, 764 (1994).
 13. Hu, Y. and Huang. C.-H., "Computer simulation of the field emission properties of multiwalled carbon nanotubes for flat panel displays," *J. Vac. Sci. Technol. B* **21**, 1648 (2003).
 14. Iannazzo, S., "A SURVER OF THE PRESENT STATUS OF VACUUM MICROELECTRONICS," *Solid-State Electronics* **36**, 301 (1993).
 15. Iijima, S., "Helical microtubules of graphitic carbon," *Nature* **354**, 56 (1991).



16. Iijima, S. and Ichihashi, T., "Single-shell carbon nanotubes of 1-nm diameter," Nature **363**, 603 (1993).
17. Itoh, S., Niiyama, T., and Yokoyama, M., "Influences of gases on the field emission," J. Vac. Sci. Technol. B **11**, 647 (1993).
18. Itoh, S., Tanaka, M., and Tonegawa, T., "Development of field emission displays," J. Vac. Sci. Technol. B **22**, 1362 (2004).
19. Lan, Y.-C., Lai, J.-T., Chen, S.-H., Wang, W.-C., Tsai, C.-H., Tsai, K.-L., and Sheu, C.-Y., "Simulation of focusing field emission devices," J. Vac. Sci. Technol. B **18**, 911 (2000).
20. Lan, Y.-C., Lee, C.-T., Hu, Y., Chen, S.-H., Lee, C.-C., Tsui, B.-Y., and Lin, T.-L., "Simulation study of carbon nanotube field emission display with under-gate and planar-gate structures," J. Vac. Sci. Technol. B **22**, 1244 (2004).
21. Lei, W., Wang, B., and Yin, H., "Simulation study on performance of field emitter array," J. Vac. Sci. Technol. B **16**, 2881 (1998).
22. Lian, Y.-Y., *Parallel Three-Dimensional Direct Simulation Monte Carlo Method and Its Applications*, pp.9 (2001).
23. Meyer, R., Ghis, A., Rambaud, P., and Muller, F., Technical Digest of Japan Display'86, 513 (1986).
24. Nilsson, L., Groening, O., Emmenegger, C., Kuettel, O., Schaller, E.,

- Schlapbach, L., Kind, H., Bonard, J. M. and Kern, K., "Scanning field emission from patterned carbon nanotube films," *Appl. Phys. Lett.* **76**, 2071 (2000).
25. Pirio, G, Legagneux, P., Pribat, D., Teo, K. B. K., Chhowalla, M., Amaratunga, G. A. J., and Milne, W. I., "Fabrication and electrical characteristics of carbon nanotube field emission microcathodes with an integrated gate electrode," *Nanotechnology* **13**, 1 (2002).
26. Rao, A. M., Jacques, D., and Haddon, R. C., Zhu, W., Bower, C., and Jin, S., "In situ-grown carbon nanotube array with excellent field emission characteristics," *Appl. Phys. Lett.* **76**, 3813 (2000).
27. Saad, Yousef, *Iterative Methods for Sparse Linear Systems*, PWS Publishing Company, International Edition (1996).
28. Shoulders, K. R., *Adv. Computers* **2**, 135 (1961).
29. Spindt, C. A., "A Thin-Film Field-Emission Cathode," *J. Appl. Phys.* **39**, 3504 (1968).
30. Spindt, C. A., Brodie, I., Humphrey, L., and Westerberg, E. R., "Physical properties of thin-film field emission cathodes with molybdenum cones," *J. Appl. Phys.* **47**, 5248 (1976).
31. T.W. Odom, J.-L. Huang, P. Kim, and C. M. Lieber, "Atomic structure and

- electronic properties of single-walled carbon nanotubes,” *Nature* **391**, 62 (1998).
32. Wang, C., Wang, B. and Zhao, Z., “Numerical modeling of the disk-edge field emitter triode,” *J. Vac. Sci. Technol. B* **15**, 394 (1997).
33. Wang, Q. H., Corrigan, T. D., Dai, J. Y., and Chang, R. P. H., “Field emission from nanotube bundle emitters at low fields,” *Appl. Phys. Lett.* **70**, 3308 (1997).
34. Wildoer, J.W.G., Venema, L. C., Rinzler, A. G., Smally, R. E., and Dekker, C., “Electronic structure of atomically resolved carbon nanotubes,” *Nature* **391**, 59 (1998).



Appendix A

3D Poisson solver formulation via FEM

$$\nabla^2 \varphi = -\frac{\rho}{\varepsilon_0}$$

For the element equation,

$$\iiint \phi_i^{(e)} \left(\frac{\partial^2 \varphi^{(e)}}{\partial x^2} + \frac{\partial^2 \varphi^{(e)}}{\partial y^2} + \frac{\partial^2 \varphi^{(e)}}{\partial z^2} \right) dx dy dz = -\iiint \left(\frac{\rho}{\varepsilon_0} \right) \phi_i^{(e)} dx dy dz$$

Integrated by part with following formulas,

$$\phi_i^{(e)} \frac{\partial^2 \varphi^{(e)}}{\partial x^2} = \frac{\partial}{\partial x} \left(\phi_i^{(e)} \frac{\partial \varphi^{(e)}}{\partial x} \right) - \frac{\partial \phi_i^{(e)}}{\partial x} \frac{\partial \varphi^{(e)}}{\partial x}$$

$$\phi_i^{(e)} \frac{\partial^2 \varphi^{(e)}}{\partial y^2} = \frac{\partial}{\partial y} \left(\phi_i^{(e)} \frac{\partial \varphi^{(e)}}{\partial y} \right) - \frac{\partial \phi_i^{(e)}}{\partial y} \frac{\partial \varphi^{(e)}}{\partial y}$$

$$\phi_i^{(e)} \frac{\partial^2 \varphi^{(e)}}{\partial z^2} = \frac{\partial}{\partial z} \left(\phi_i^{(e)} \frac{\partial \varphi^{(e)}}{\partial z} \right) - \frac{\partial \phi_i^{(e)}}{\partial z} \frac{\partial \varphi^{(e)}}{\partial z}$$

Therefore,

$$\begin{aligned} & \iiint \left[\frac{\partial}{\partial x} \left(\frac{\partial \varphi^{(e)}}{\partial x} \phi_i^{(e)} \right) + \frac{\partial}{\partial y} \left(\frac{\partial \varphi^{(e)}}{\partial y} \phi_i^{(e)} \right) + \frac{\partial}{\partial z} \left(\frac{\partial \varphi^{(e)}}{\partial z} \phi_i^{(e)} \right) \right] dx dy dz \\ & - \iiint \left[\left(\frac{\partial \varphi^{(e)}}{\partial x} \frac{\partial \phi_i^{(e)}}{\partial x} \right) + \left(\frac{\partial \varphi^{(e)}}{\partial y} \frac{\partial \phi_i^{(e)}}{\partial y} \right) + \left(\frac{\partial \varphi^{(e)}}{\partial z} \frac{\partial \phi_i^{(e)}}{\partial z} \right) \right] dx dy dz \\ & = -\iiint \left(\frac{\rho}{\varepsilon_0} \right) \phi_i^{(e)} dx dy dz \end{aligned}$$

Using Gauss divergence theorem,

$$\begin{aligned} & \iint_A \phi_i^{(e)} \left(\frac{\partial \varphi^{(e)}}{\partial x} \bar{i} + \frac{\partial \varphi^{(e)}}{\partial y} \bar{j} + \frac{\partial \varphi^{(e)}}{\partial z} \bar{k} \right) \cdot \bar{u} dA \\ & - \iiint \left[\left(\frac{\partial \varphi^{(e)}}{\partial x} \frac{\partial \phi_i^{(e)}}{\partial x} \right) + \left(\frac{\partial \varphi^{(e)}}{\partial y} \frac{\partial \phi_i^{(e)}}{\partial y} \right) + \left(\frac{\partial \varphi^{(e)}}{\partial z} \frac{\partial \phi_i^{(e)}}{\partial z} \right) \right] dx dy dz \\ & = -\iiint \left(\frac{\rho}{\varepsilon_0} \right) \phi_i^{(e)} dx dy dz \end{aligned}$$

we let

$$\bar{\tau}^{(e)} = -\left(\frac{\partial \varphi^{(e)}}{\partial x} \bar{i} + \frac{\partial \varphi^{(e)}}{\partial y} \bar{j} + \frac{\partial \varphi^{(e)}}{\partial z} \bar{k} \right)$$

and equation can be rewritten as follows:

$$\iiint \left[\left(\frac{\partial \varphi^{(e)}}{\partial x} \frac{\partial \phi_i^{(e)}}{\partial x} \right) + \left(\frac{\partial \varphi^{(e)}}{\partial y} \frac{\partial \phi_i^{(e)}}{\partial y} \right) + \left(\frac{\partial \varphi^{(e)}}{\partial z} \frac{\partial \phi_i^{(e)}}{\partial z} \right) \right] dx dy dz$$

$$= \iiint \left(\frac{\rho}{\varepsilon_0} \right) \phi_i^{(e)} dx dy dz - \iint_A \phi_i^{(e)} \tau_u^{(e)} dA$$

we let the trial solution

$$\varphi^{(e)}(x, y, z; a) = \sum_{j=1}^4 a_j \phi_j(x, y, z)$$

where

$$\phi_i(x, y, z) = \frac{1}{6V} (a_i^* + b_i^* x + c_i^* y + d_i^* z)$$

$$a_i^* = \begin{vmatrix} x_k & y_k & z_k \\ x_l & y_l & z_l \\ x_m & y_m & z_m \end{vmatrix} \quad b_i^* = - \begin{vmatrix} 1 & y_k & z_k \\ 1 & y_l & z_l \\ 1 & y_m & z_m \end{vmatrix}$$

$$c_i^* = - \begin{vmatrix} x_k & 1 & z_k \\ x_l & 1 & z_l \\ x_m & 1 & z_m \end{vmatrix} \quad d_i^* = - \begin{vmatrix} x_k & y_k & 1 \\ x_l & y_l & 1 \\ x_m & y_m & 1 \end{vmatrix}$$

finally,

$$\frac{1}{36V^2} \sum_{i=1}^4 \sum_{j=1}^4 \left[\iiint \left(\frac{\partial \phi_i^{(e)}}{\partial x} \frac{\partial \phi_j^{(e)}}{\partial x} + \frac{\partial \phi_i^{(e)}}{\partial y} \frac{\partial \phi_j^{(e)}}{\partial y} + \frac{\partial \phi_i^{(e)}}{\partial z} \frac{\partial \phi_j^{(e)}}{\partial z} \right) dx dy dz \right] a_j$$

$$= \iiint \left(\frac{\rho}{\varepsilon_0} \right) \phi_i^{(e)} dx dy dz - \iint_A \phi_i^{(e)} \tau_u^{(e)} dA$$

Appendix B

Grid test data

Min size	electrons	Max En	cells	nodes	File name
0.515 nm	0.10049	10.97428	53270	11045	5101
0.252 nm	0.12586	11.2486	60576	12523	5102
0.138 nm	0.13992	11.42104	67323	13906	5103
0.079 nm	0.14892	11.46701	70718	14659	5104
0.047 nm	0.15215	11.81443	85566	17619	5105
0.028 nm	0.15758	11.90023	89080	18429	5106

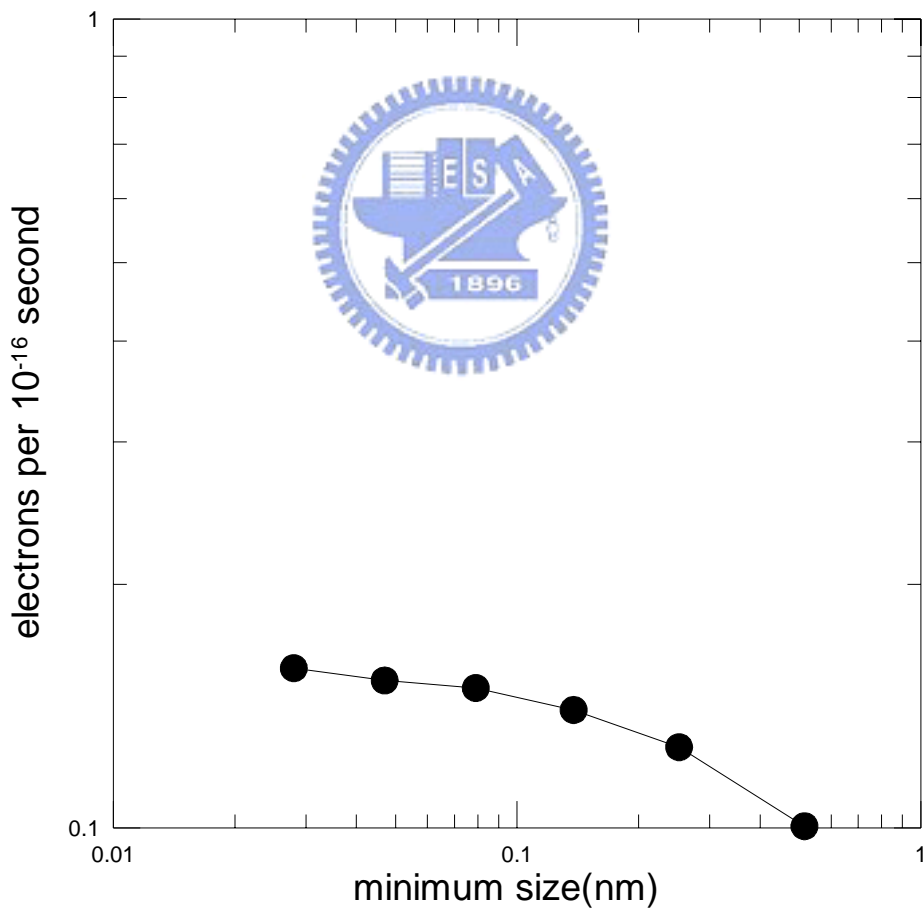


Table I. A FED has excellent features:

1.	Thin panel thickness (~2mm)
2.	Self-emissive
3.	Distortion free image
4.	Wide viewing angle (~170 °)
5.	Quick response in the order of μs by controlling with analog or digital without active elements
6.	Tolerance to environment as high as that of receiving tubes
7.	Free from the terrestrial magnetic effect
8.	Free from the changes in the ambient magnetism
9.	Quick start of operation
10.	Less dead space of images
11.	Low power consumption display device
12.	Good stable characteristics in severe environmental conditions

Table II. Classification of FEDs with the structure

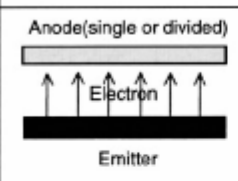
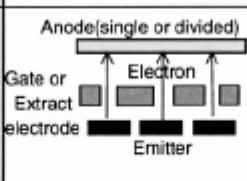
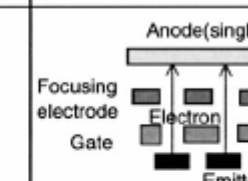
	Diode	Triode	Tetrode
Structure			
Feature	<ul style="list-style-type: none"> • Panel structure is most simple. • Anode Voltage is extract voltage. • Switching Voltage is high. 	<ul style="list-style-type: none"> • Anode and Cathode selection. • No focus electrode. • Easy fabrication for narrow gap. • Limitation for definition and luminance by beam spread. 	<ul style="list-style-type: none"> • Complicated panel Structure by inserting of focusing electrode. • High Brightness.



Table III. Triode-type without space-charge effect (silicon)

Silicon height=1000nm	Emission current form Tip	Gate current	Anode current
160V	3.44928E-5	0	3.44928E-5
150V	1.74976E-5	0	1749.76E-8
140V	8.2688E-6	0	8.2688E-6
130V	3.344E-6	0	1.30625E-5
120V	1.1872E-6	0	1.1872E-6

Table IV. Triode-type without space-charge effect (CNT 600nm)

CNT height=600nm	Emission current form CNT	Gate current	Anode current
160V	1.37296E-4	0	1.37296E-4
150V	7.37056E-5	0	7.37056E-5
140V	3.65824E-5	0	3.65824E-5
130V	1.64832E-5	0	1.64832E-5
120V	6.3264E-6	0	6.3264E-6
110V	2.2256E-6	0	2.2256E-6

Table V. Triode-type without space-charge effect (CNT 400nm)

CNT hight=400nm	Emission current form CNT	Gate current	Anode current
190V	7.76544E-5	1.4112E-6	7.62432E-5
180V	4.51072E-5	6.688E-7	4.44384E-5
170V	2.46848E-5	3.136E-7	2.43712E-5
160V	1.2608E-5	1.344E-7	1.24736E-5
150V	6.04E-6	4.16E-8	5.9984E-6
140V	2.5136E-6	0	2.5136E-6
130V	1.0016E-6	0	1.0016E-6
120V	7.504E-7	0	7.504E-7
110V	1.28E-8	0	1.28E-8

Table VI. Tetrode-type without space-charge effect (CNT 600nm)

CNT height=600nm	Emission current form CNT	Gate current	Anode current
Focus 5V	2.09728E-5	3.7472E-6	1.72256E-5
Focus 0V	2.18528E-5	6.0E-6	1.58528E-5
Focus -5V	2.10624E-5	6.6016E-6	1.44608E-5

Table VII. Triode-type with space-charge effect (CNT 600nm)

CNT height=600nm	Emission current form CNT	Gate current	Anode current
150V	1.8432E-6	0	1.8432E-6
140V	1.1296E-6	0	1.1296E-6
130V	6.384E-7	0	6.384E-7
120V	3.456E-7	0	3.456E-7

Table VIII. Tetrode-type with space-charge effect (CNT 600nm)

CNT height=600nm	Emission current form CNT	Gate current	Anode current
Focus 0V	8.50133E-7	8.352E-7	1.4933E-8

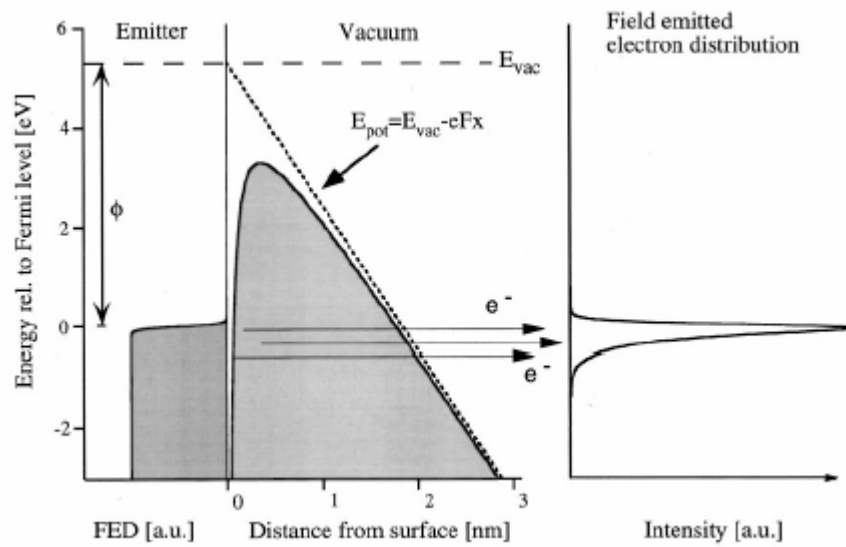


Fig. 1.1 Schematic of the situation at a surface under field emission conditions and the resulting field emission energy distribution.

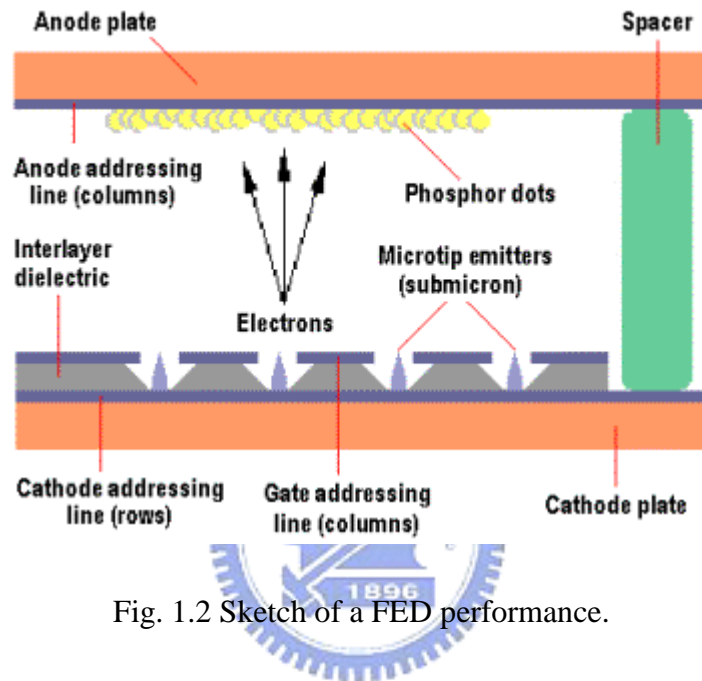


Fig. 1.2 Sketch of a FED performance.

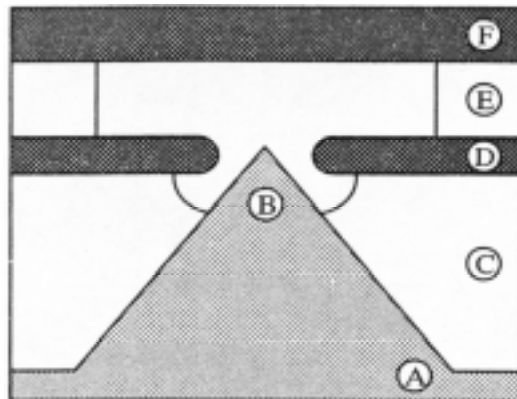
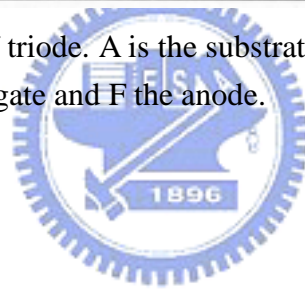


Fig. 1.3 The basic structure of triode. A is the substrate, B is the field emitter, C and E the insulating layers, D is the gate and F the anode.



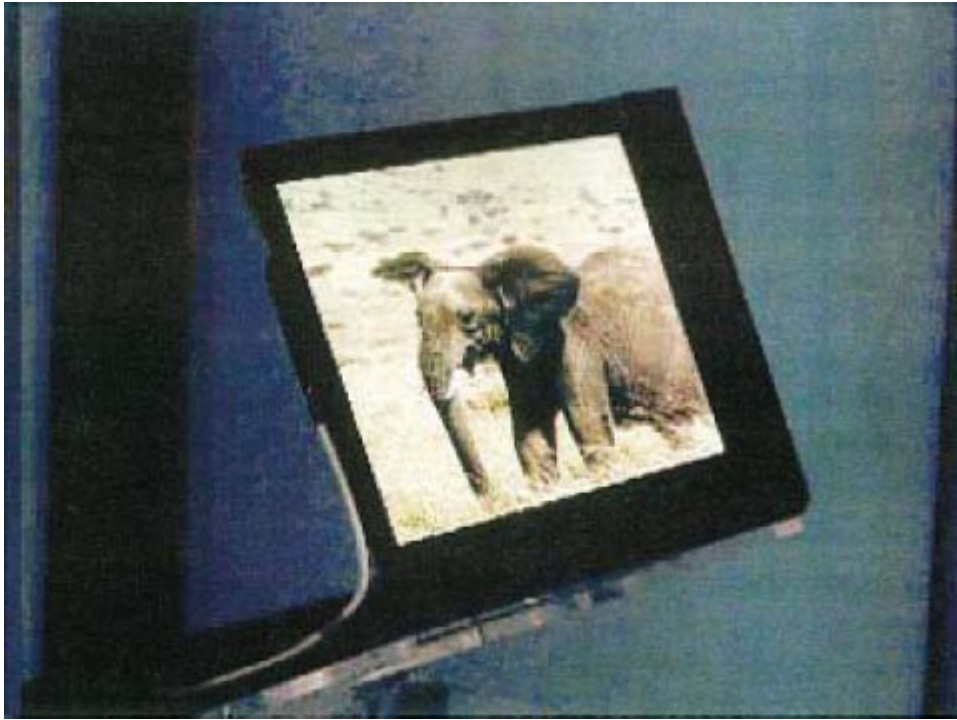


Fig. 1.4 The appearance of the 8 in. color FED panel.

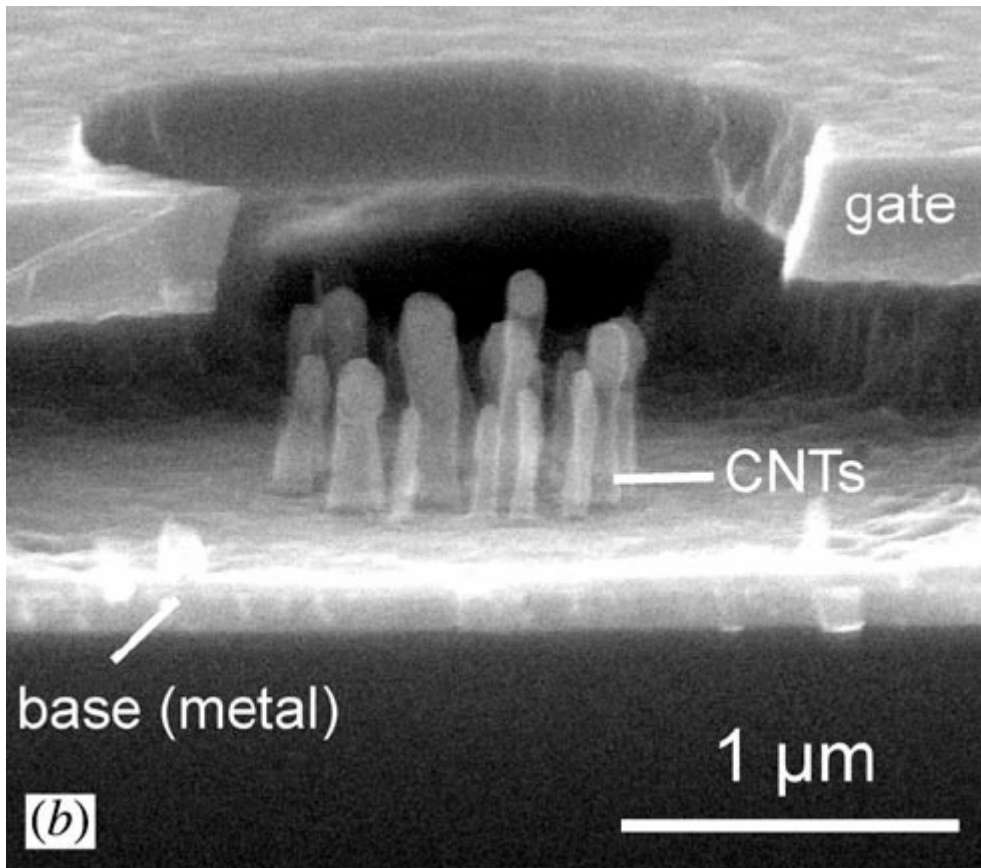


Fig. 1.5 SEM images of a microcathode.

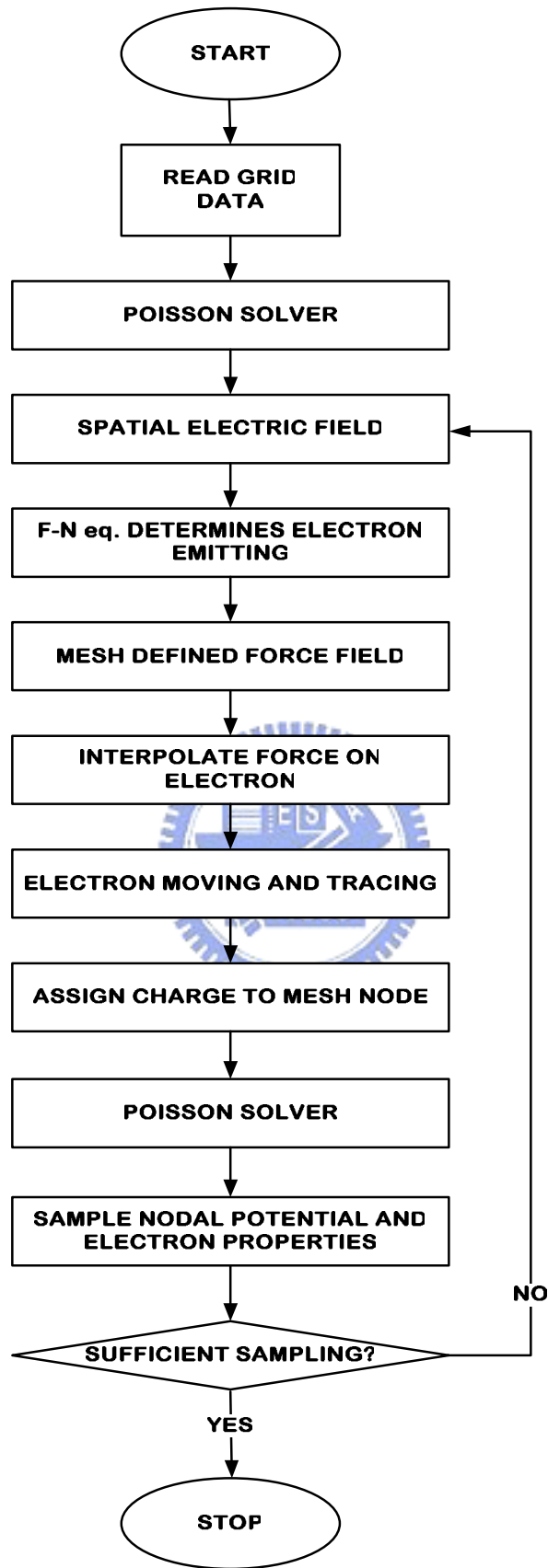


Fig. 2.1 Program flow chart.

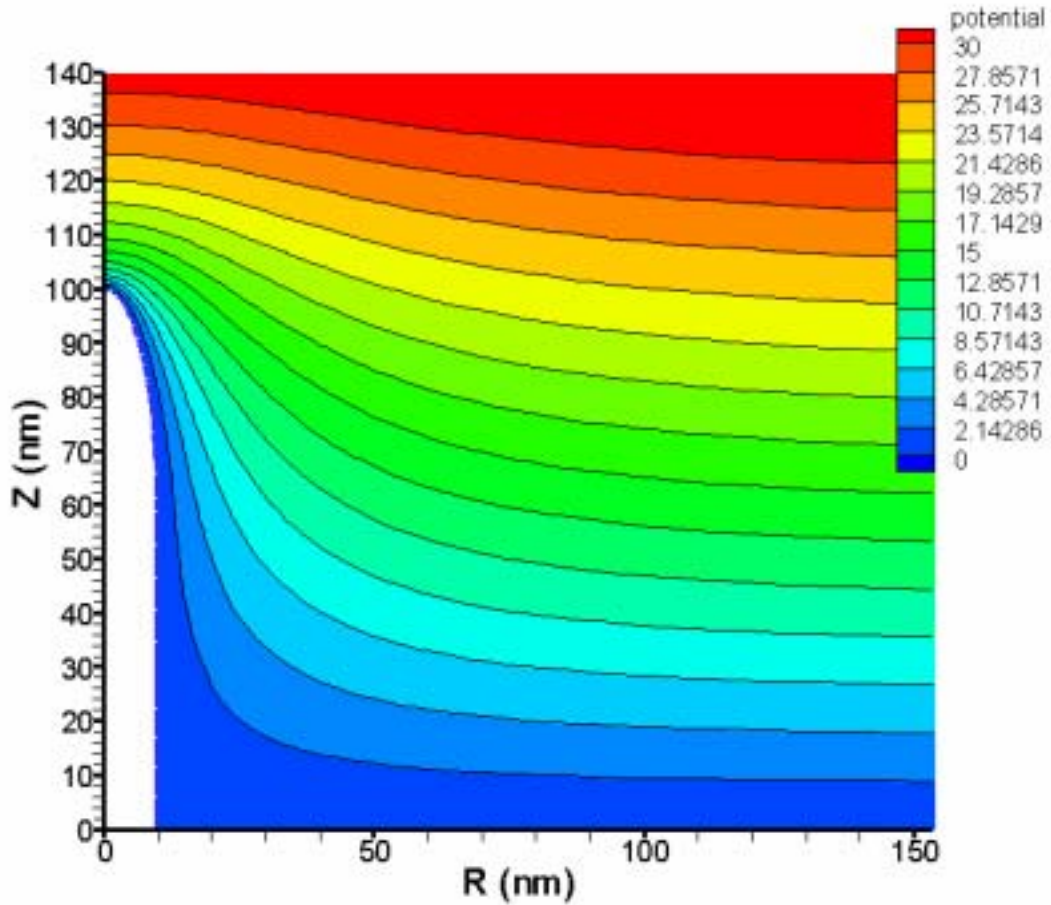


Fig. 3.1 Contour of the potential distribution around a CNT with a half-ellipsoidal tip. The simulation conditions are: applied voltage 500V, the cathode-to-anode distance $2\mu m$, radius of the simulation region $1\mu m$, major radius of the half-ellipsoidal tip 40nm, minor radius of the half-ellipsoidal tip 10nm, CNT radius 10nm, and the total CNT height 100nm.

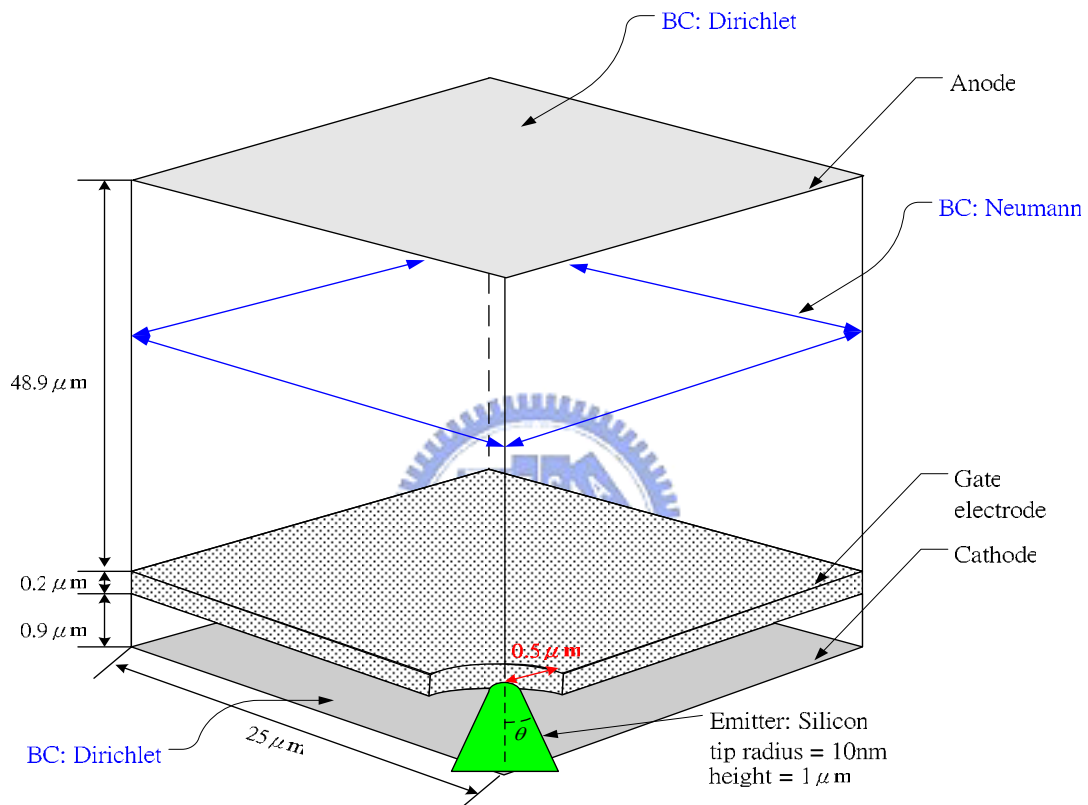


Fig. 3.2 Silicon-based emitter simulation domain. (triode-type)

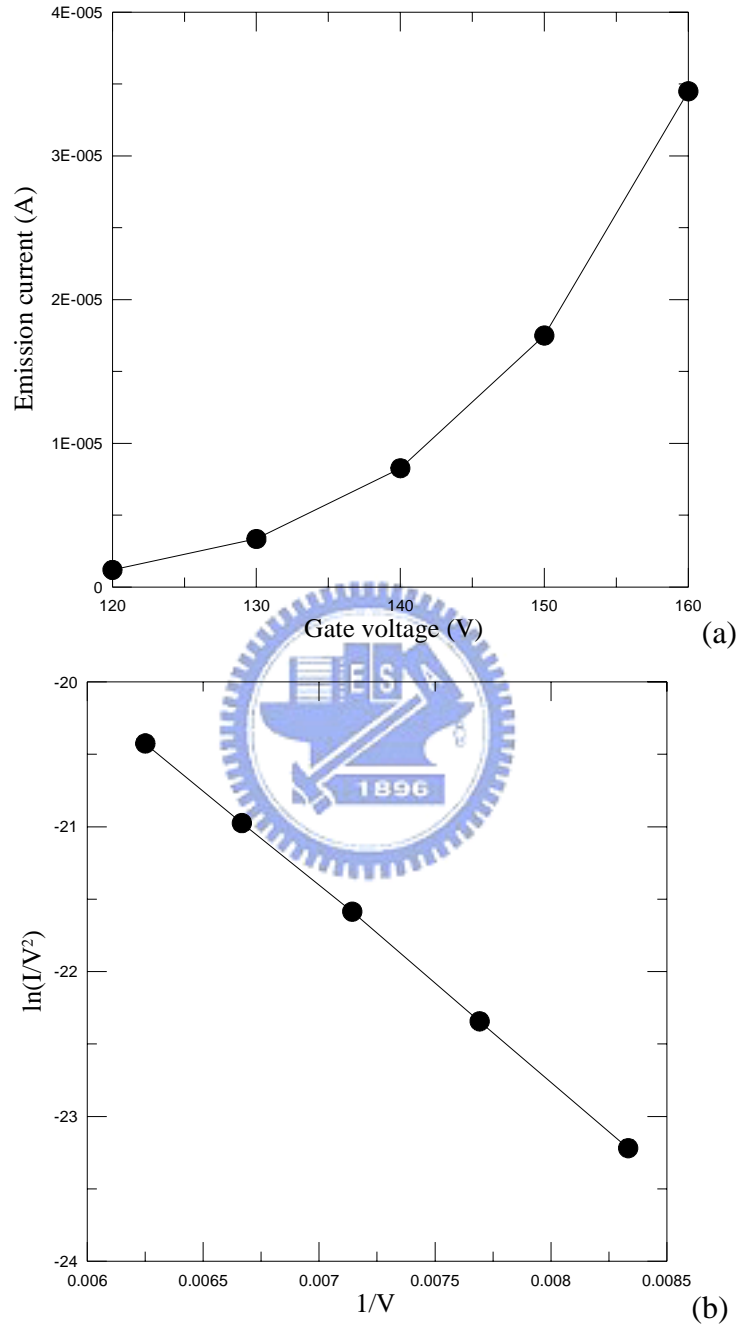


Fig. 3.3 Simulation of silicon-based emitter without space charge effect: (a) is the field emission I-V curve, and (b) shows the data plotted in Fowler-Nordheim coordinates.

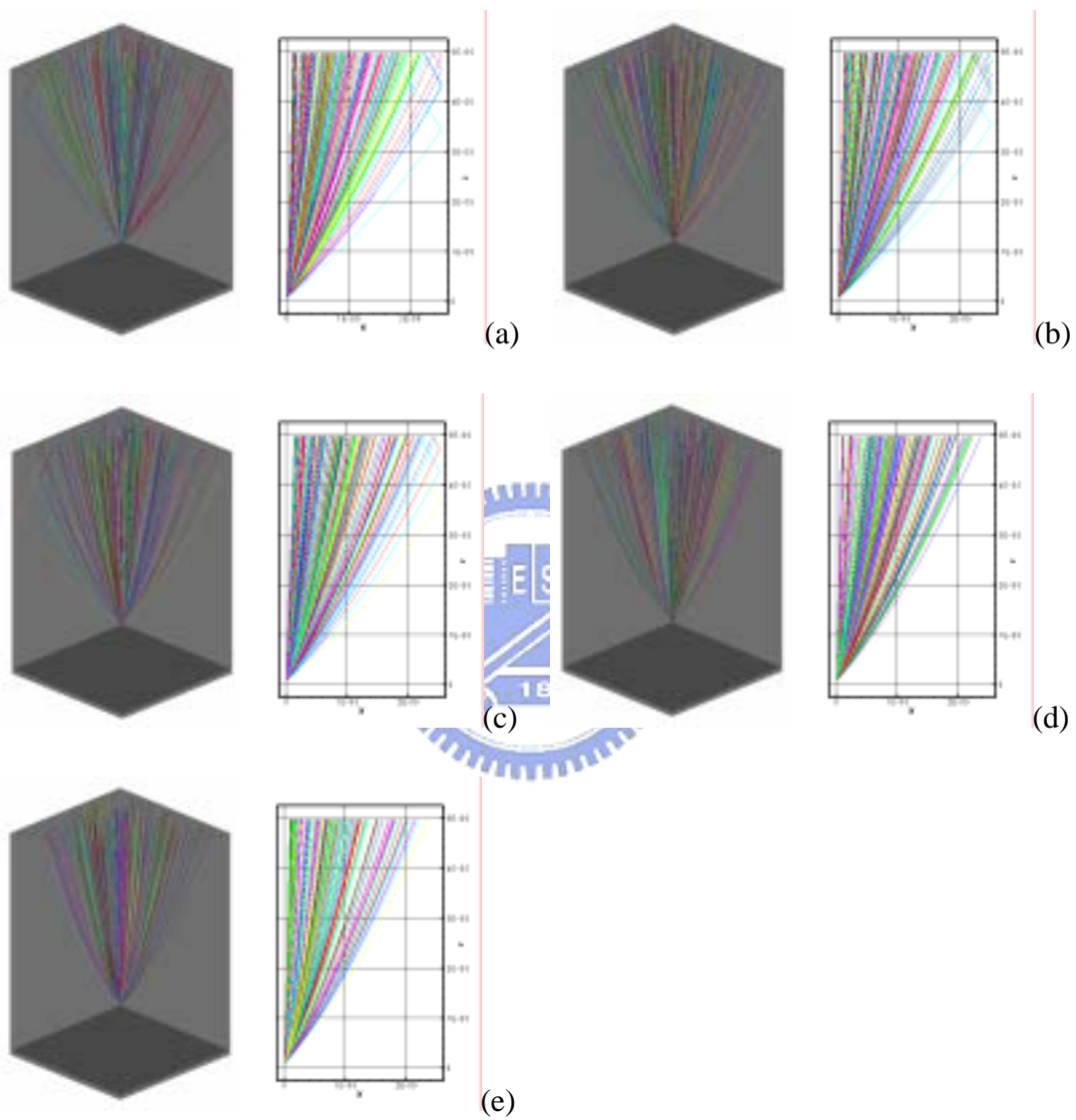


Fig. 3.4 Typical electron trajectories using PIC simulation without space charge effect (silicon-based emitter without focus electrode): (a) gate applied 160V; (b) gate applied 150V; (c) gate applied 140V; (d) gate applied 130V; (e) gate applied 120V.

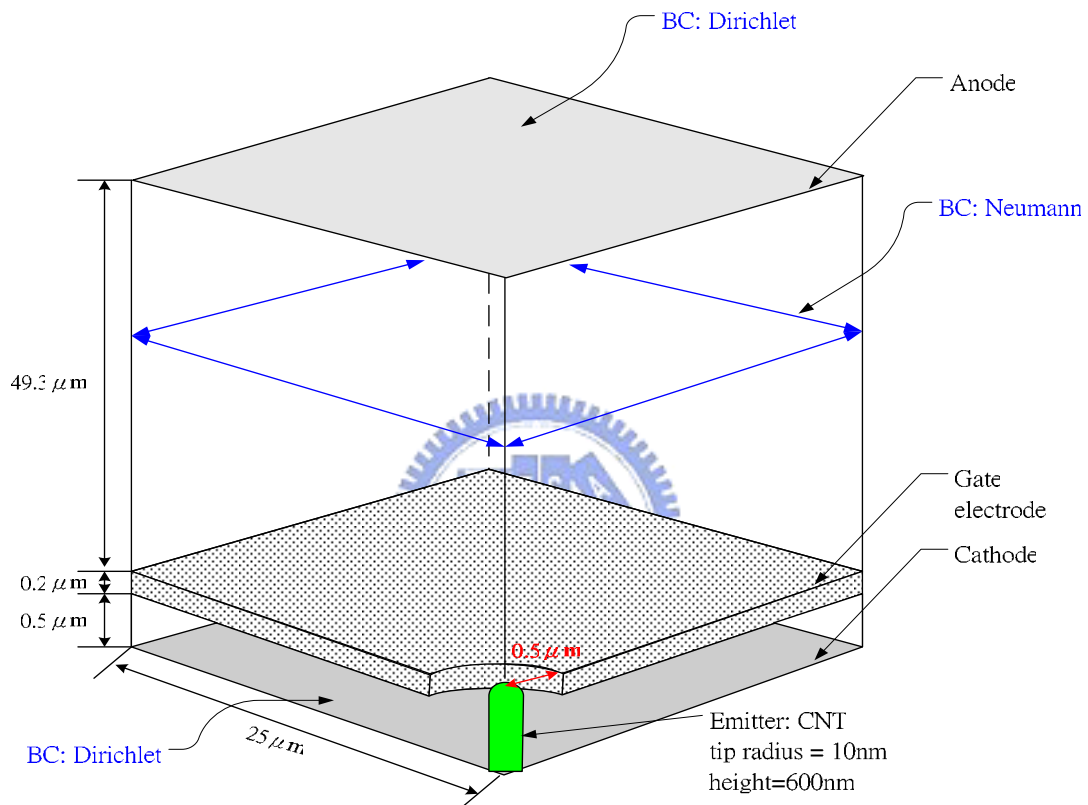


Fig. 3.5 CNT emitter simulation domain. (triode-type)

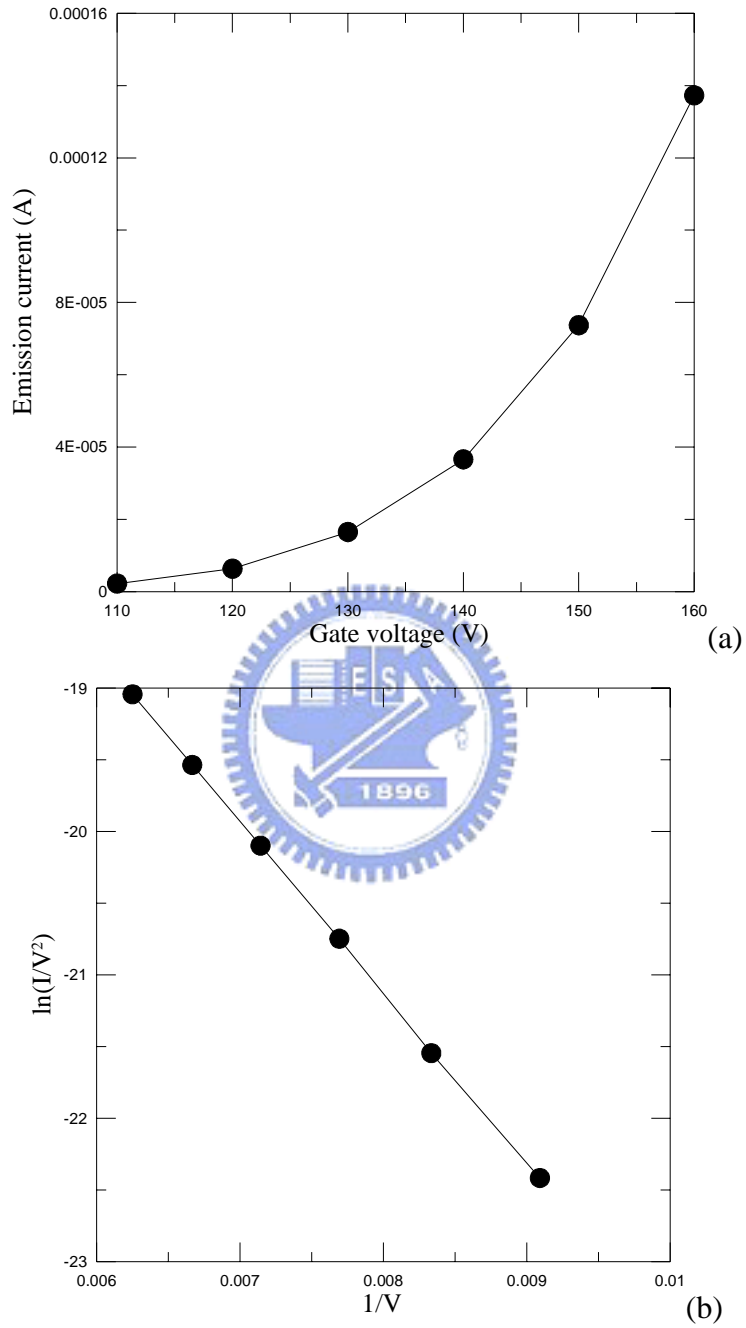


Fig. 3.6 Simulation of CNT emitter (600nm) without space charge effect: (a) is the field emission I-V curve, and (b) shows the data plotted in Fowler-Nordheim coordinates.

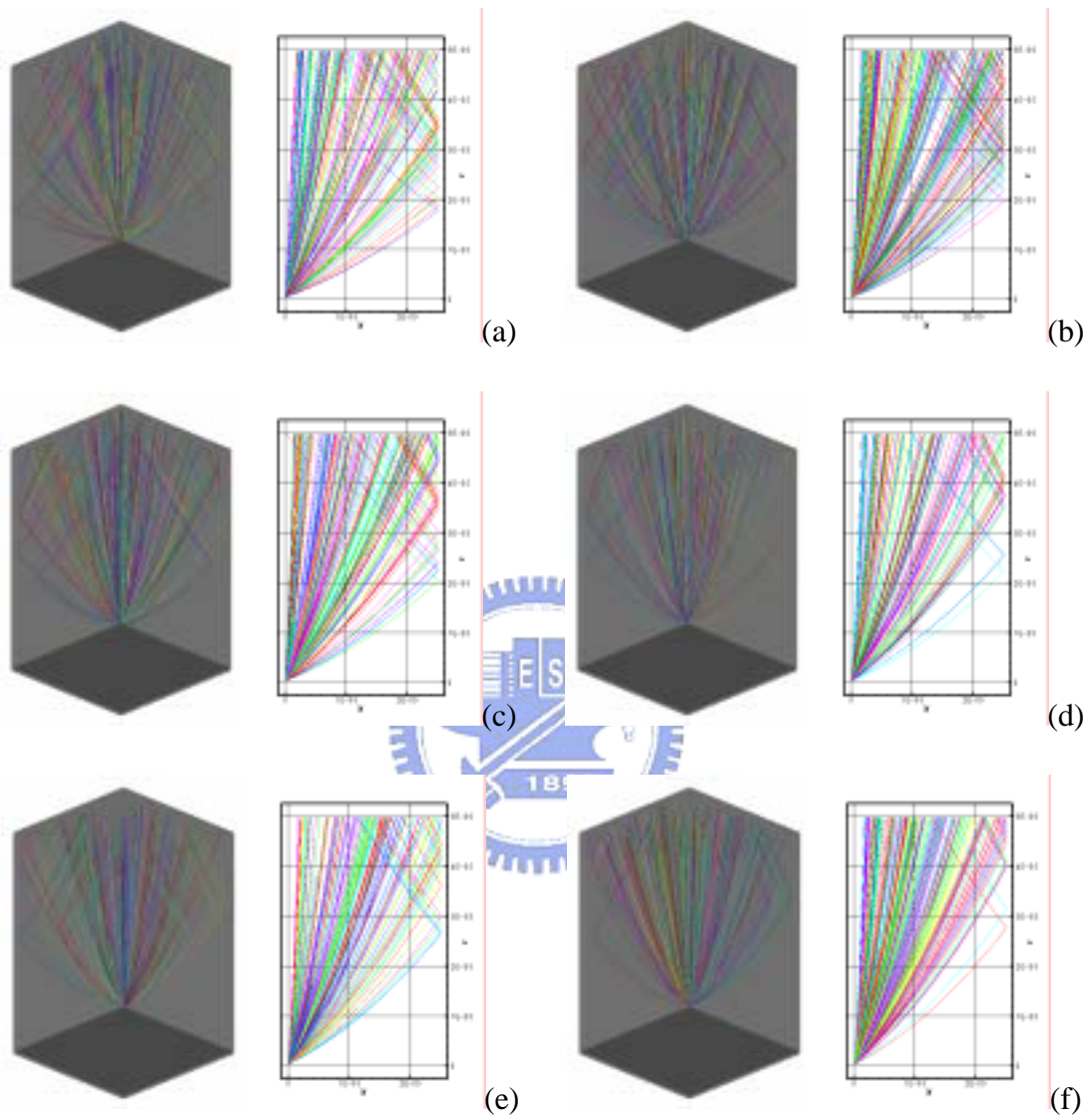


Fig. 3.7 Typical electron trajectories using PIC simulation without space charge effect (CNT emitter 600nm without focus electrode): (a) gate applied 160V; (b) gate applied 150V; (c) gate applied 140V; (d) gate applied 130V; (e) gate applied 120V; (f) gate applied 110V.

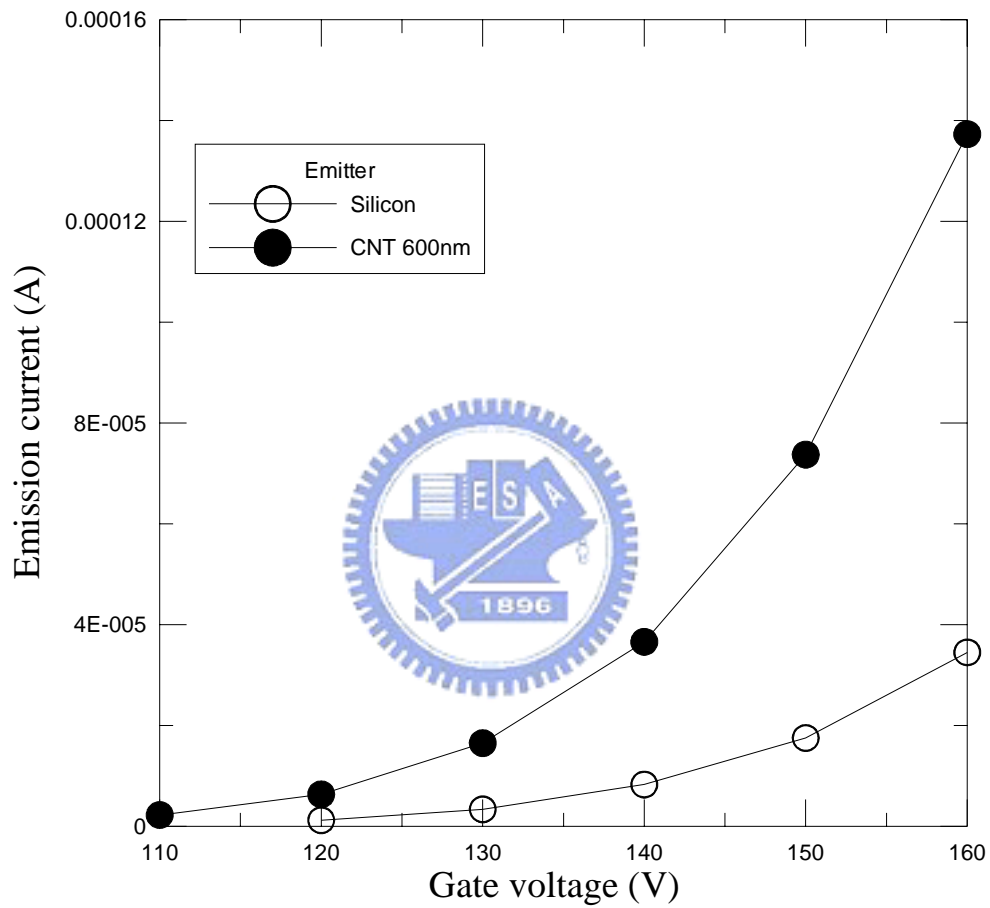


Fig. 3.8 Comparison of emission current of different material emitter. (without space charge effect)

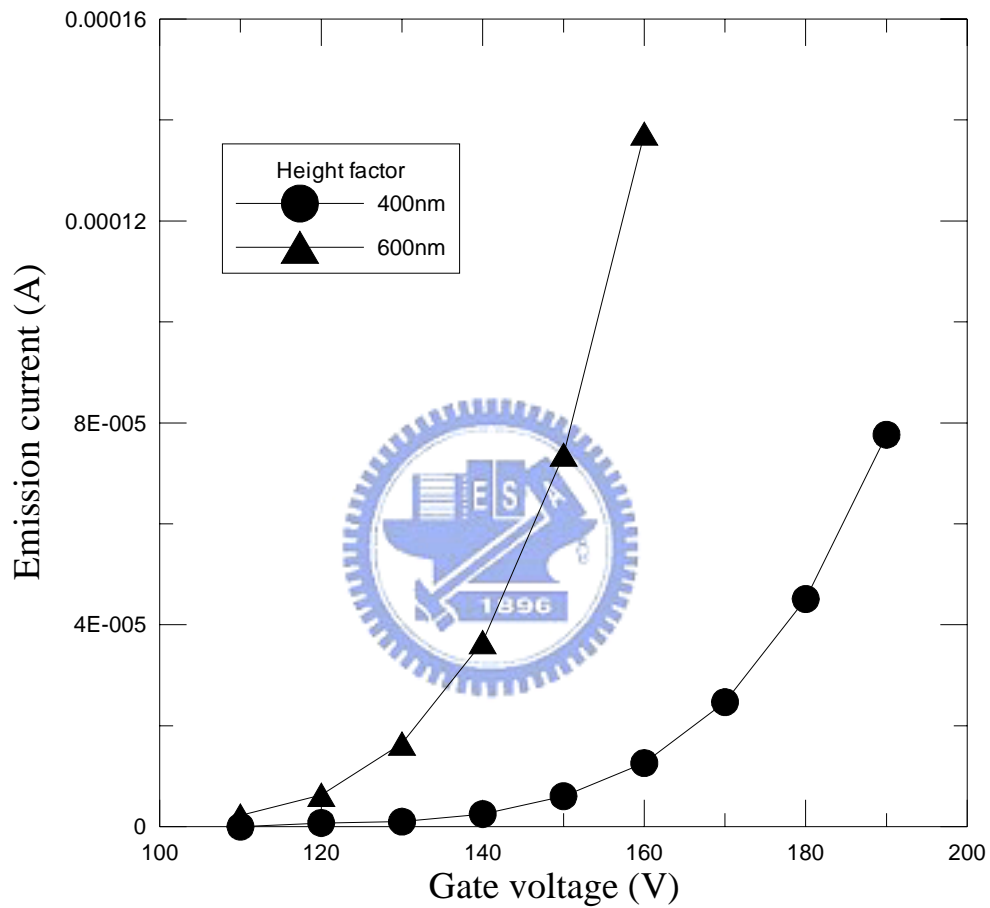


Fig. 3.9 Comparison of emission current of different emitter height. (CNT emitter without space charge effect)

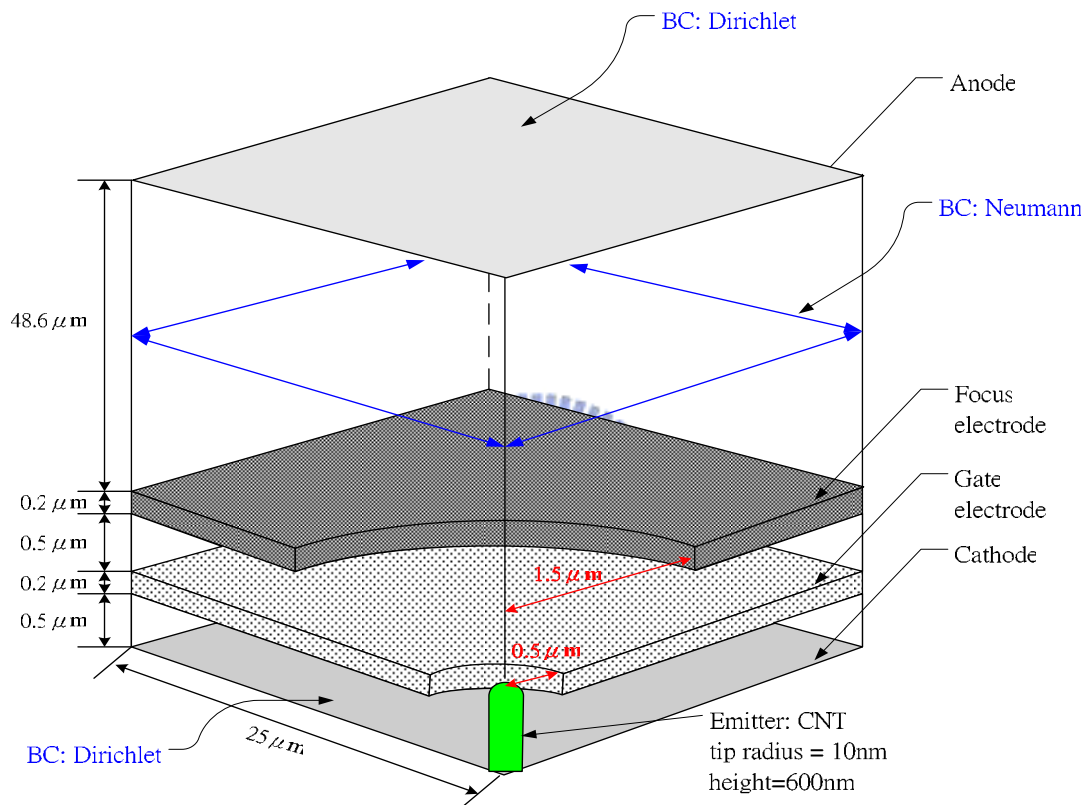


Fig. 3.10 CNT emitter simulation domain. (tetrode-type)

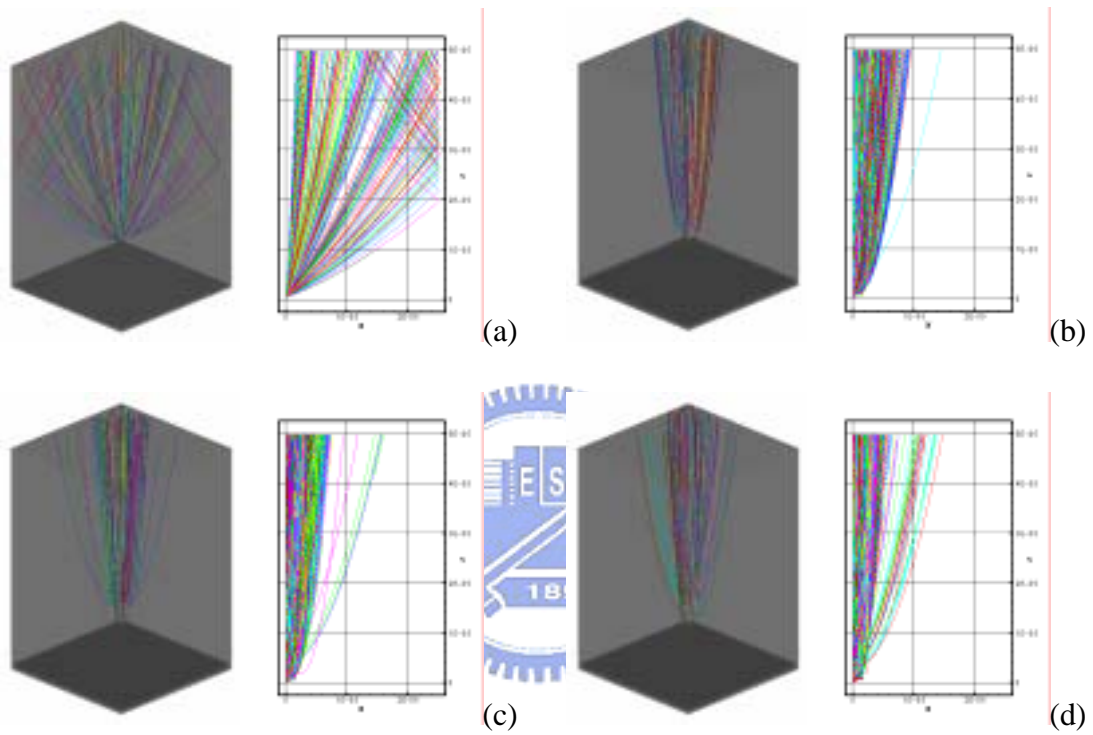


Fig. 3.11 Comparison of focusing effect simulations of CNT emitter (600nm) without space charge effect: (a) without focus electrode; (b) focus electrode applied 5V; (c) focus electrode applied 0V; (d) focus electrode applied -5V.

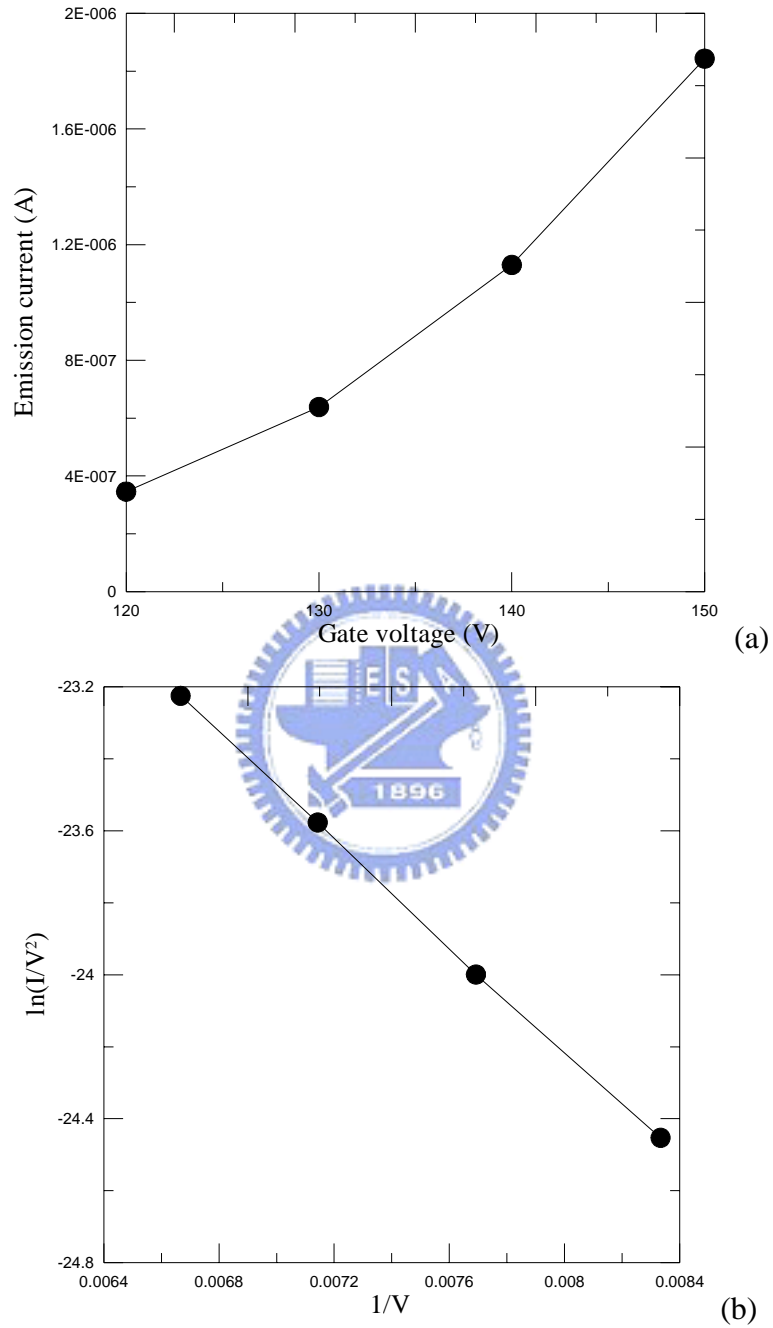


Fig. 3.12 Simulation of CNT emitter (600nm) with space charge effect: (a) is the field emission I-V curve, and (b) shows the data plotted in Fowler-Nordheim coordinates.

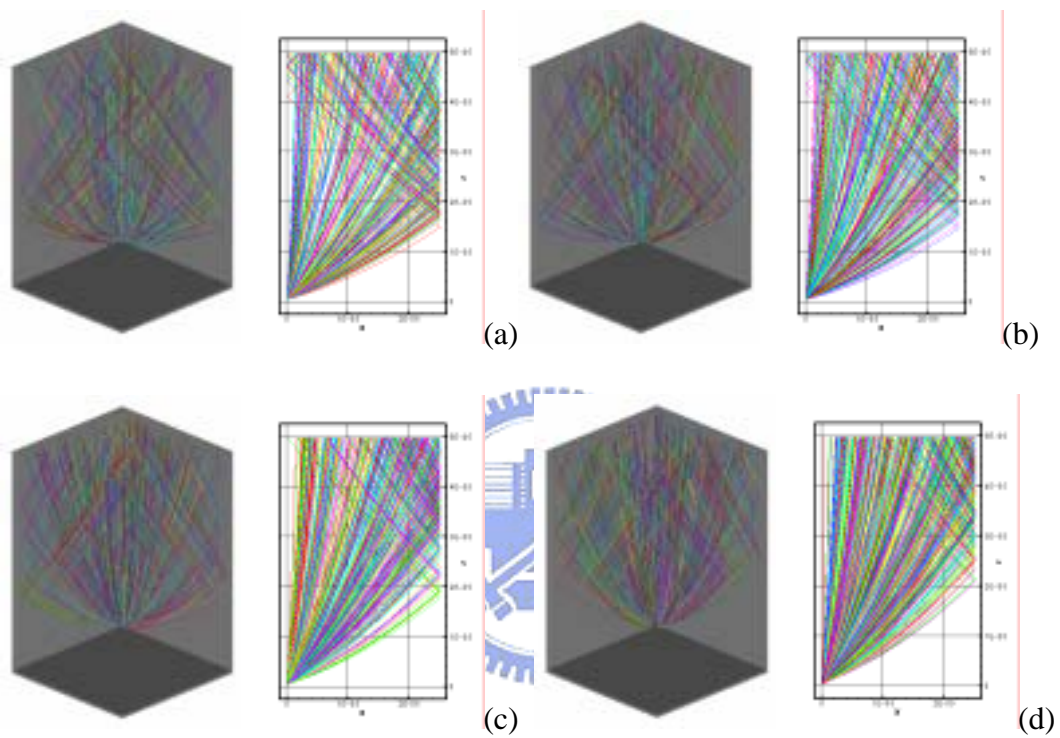


Fig. 3.13 Typical electron trajectories using PIC simulation with space charge effect (CNT emitter 600nm without focus electrode): (a) gate applied 150V; (b) gate applied 140V; (c) gate applied 130V; (d) gate applied 120V.

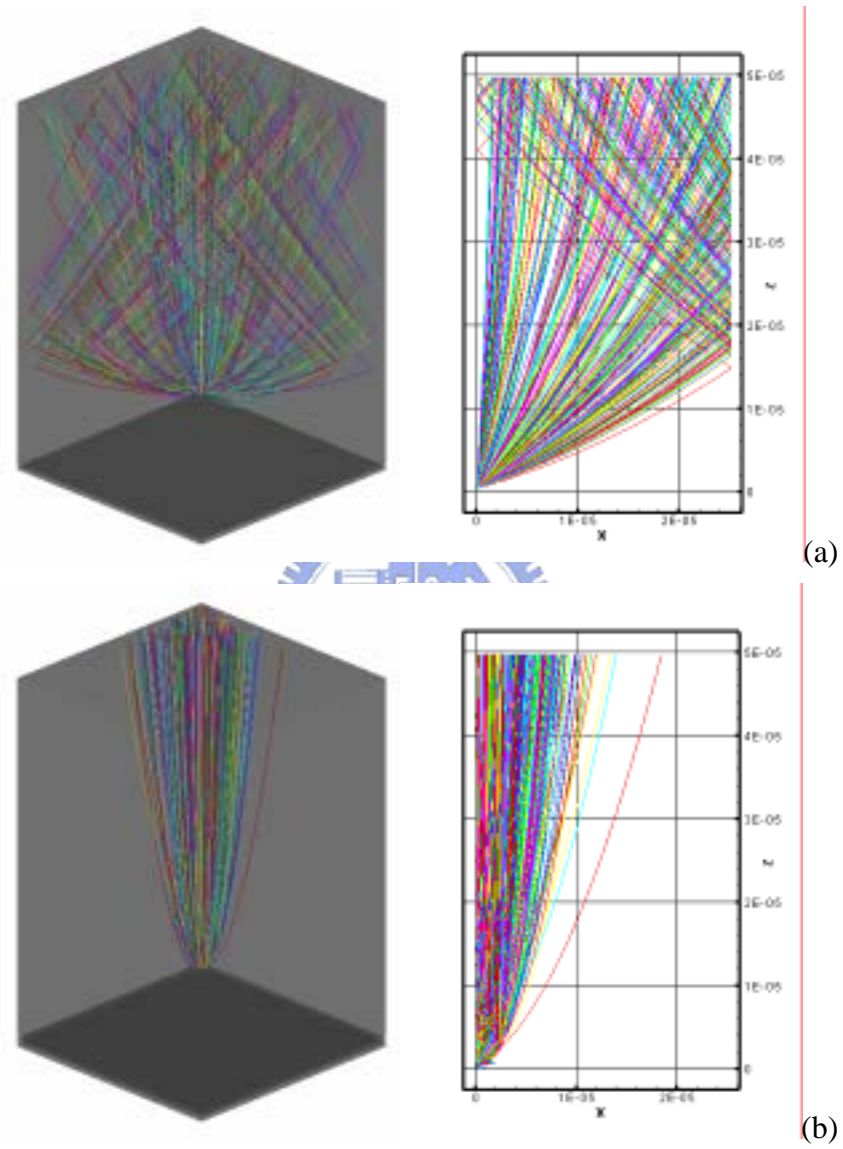


Fig. 3.14 Comparison of focusing effect simulations of CNT emitter (600nm) with space charge effect: (a) without focus electrode; (b) focus electrode applied 0V.

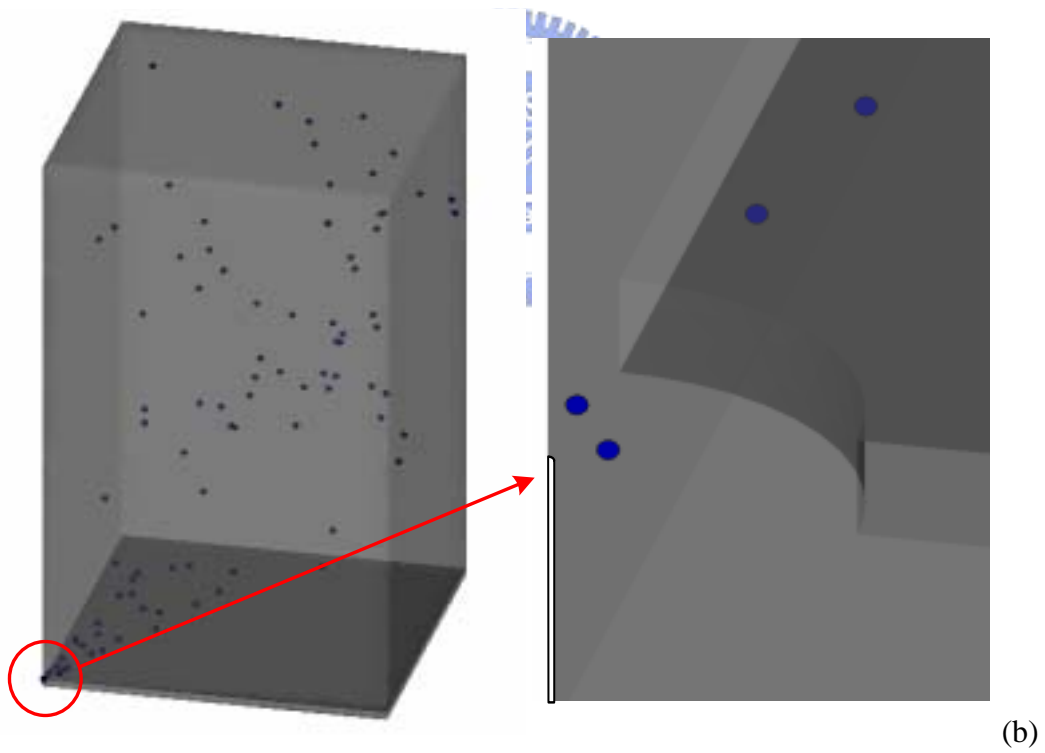
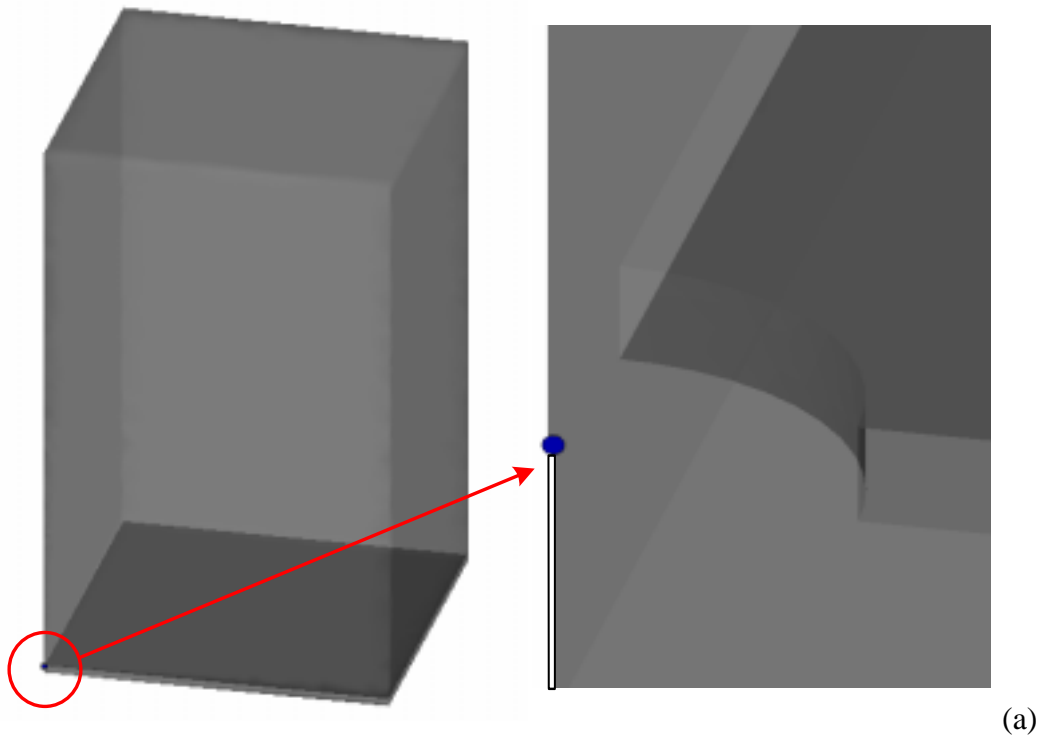


Fig. 3.15 Space charge distribution, left hand side is the full view and right hand side is the local magnification: (a) electron just leaving emitter; (b) simulation domain full of electrons.

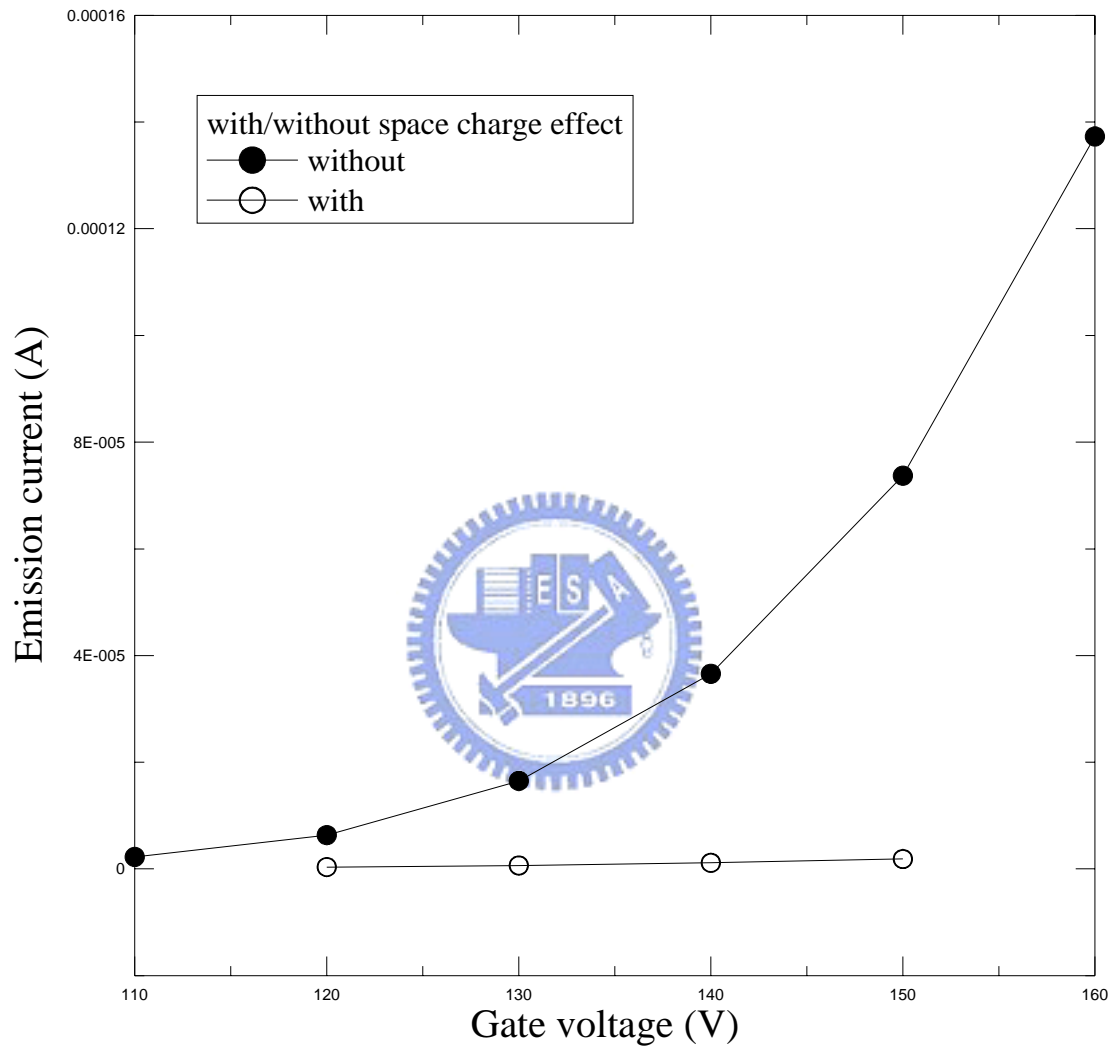


Fig. 3.16 Comparison of emission current simulations of CNT emitter (600nm): with (hollow) and without (solid) space charge effect.

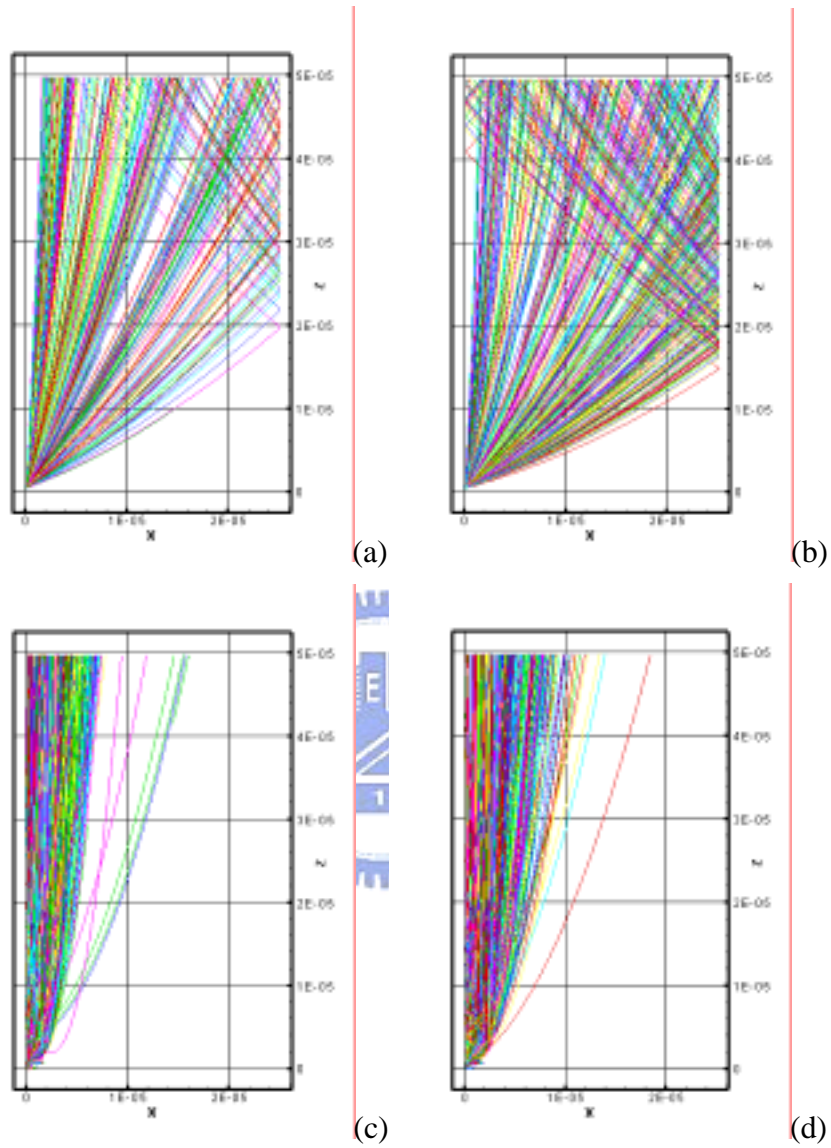


Fig. 3.17 Typical electron trajectories using PIC simulation (CNT emitter 600nm): (a) without space charge effect, without focus electrode and gate applied 150V; (b) with space charge effect, without focus electrode and gate applied 150V; (c) without space charge effect, focus applied 0V and gate applied 150V; (d) with space charge effect, focus applied 0V and gate applied 150V.